NEOPLASIA
www.neoplasia.com

Volume 13 Number 2 February 2011 pp. 81–97 **81**

Analysis of Cancer Metabolism by Imaging Hyperpolarized Nuclei: Prospects for Translation to Clinical Research

John Kurhanewicz[*,1], Daniel B. Vigneron[*,1], Kevin Brindle[†], Eduard Y. Chekmenev[‡], Arnaud Comment[§], Charles H. Cunningham[¶], Ralph J. DeBerardinis[#], Gary G. Green[**], Martin O. Leach[††], Sunder S. Rajan[‡‡], Rahim R. Rizi[§§], Brian D. Ross[¶¶], Warren S. Warren[##] and Craig R. Malloy[*,1]**

*Department of Radiology and Biomedical Imaging, University of California at San Francisco, San Francisco, CA, USA; [†]Department of Biochemistry, University of Cambridge, Cambridge, UK; [‡]Department of Radiology, Vanderbilt University, Nashville, TN, USA; [§]Laboratory for Functional and Metabolic Imaging, Ecole Polytechnique Fédérale De Lausanne, Lausanne, Switzerland; [¶]Sunnybrook Health Sciences Centre, University of Toronto, Toronto, Canada; [#]Department of Pediatrics, UT Southwestern Medical Center, Dallas, TX, USA; **York Neuroimaging Center, University of York, York, UK; [††]Royal Marsden Hospital, The Institute of Cancer Research, London, UK; [‡‡]Center for Devices and Radiological Health, FDA, White Oak, MD, USA; [§§]Department of Radiology, University of Pennsylvania, Philadelphia, PA, USA; [¶¶]Department of Magnetic Resonance Spectroscopy, Huntington Medical Research Institute, Pasadena, CA, USA; [##]Department of Chemistry, Duke University, Durham, NC, USA; ***Advanced Imaging Research Center, UT Southwestern Medical Center and VA North Texas Healthcare System, Dallas, TX, USA

Abstract

A major challenge in cancer biology is to monitor and understand cancer metabolism *in vivo* with the goal of improved diagnosis and perhaps therapy. Because of the complexity of biochemical pathways, tracer methods are required for detecting specific enzyme-catalyzed reactions. Stable isotopes such as ^{13}C or ^{15}N with detection by nuclear magnetic resonance provide the necessary information about tissue biochemistry, but the crucial metabolites are present in low concentration and therefore are beyond the detection threshold of traditional magnetic resonance methods. A solution is to improve sensitivity by a factor of 10,000 or more by temporarily redistributing the populations of nuclear spins in a magnetic field, a process termed *hyperpolarization*. Although this effect is short-lived, hyperpolarized molecules can be generated in an aqueous solution and infused *in vivo* where metabolism generates products that can be imaged. This discovery lifts the primary constraint on magnetic resonance imaging for monitoring metabolism—poor

Address all correspondence to: Prof. John Kurhanewicz, Department of Radiology and Biomedical Imaging, University of California at San Francisco Mission Bay Campus, Byers Hall, Room 203E, 1700 4th St, San Francisco, CA 94158-2330. E-mail: John.Kurhanewicz@radiology.ucsf.edu
[1]Lead authors.
Received 2 August 2010; Revised 18 October 2010; Accepted 22 October 2010

DOI 10.1593/neo.101102

sensitivity—while preserving the advantage of biochemical information. The purpose of this report was to briefly summarize the known abnormalities in cancer metabolism, the value and limitations of current imaging methods for metabolism, and the principles of hyperpolarization. Recent preclinical applications are described. Hyperpolarization technology is still in its infancy, and current polarizer equipment and methods are suboptimal. Nevertheless, there are no fundamental barriers to rapid translation of this exciting technology to clinical research and perhaps clinical care.

Neoplasia (2011) 13, 81–97

Introduction

Our understanding of cancer biology and our ability to image malignancies have evolved radically in the past 40 years. Each major step forward in cancer imaging was achieved by advances across multiple fields including physics, chemistry, medicine, and computation. Despite these successes, cancer imaging still lacks reliability in providing key biologic information about the tumor—its genetics, clinical stage, rate of growth, response to therapy, and others—underscoring the continued need for novel approaches. Recently, dramatic improvements in our ability to image specific molecules have been demonstrated using magnetic resonance imaging (MRI) of molecules prepared by a process termed *hyperpolarization*. Imaging hyperpolarized nuclei again presents the fields of oncology and medical imaging with an opportunity to dramatically improve our ability to identify and understand tumor tissue. In addition to the absence of ionizing radiation and convenient integration with standard MRI, imaging hyperpolarized nuclei offers the prospect of monitoring tumor metabolism essentially noninvasively. Imaging of hyperpolarized ^{13}C-labeled substrates has attracted particular interest because, unlike any other imaging technology, the products of metabolism in a specific enzyme-catalyzed reaction may be observed based on inherent MR frequency differences.

In this report, we provide a brief survey of our understanding of cancer metabolism, the current role of positron tomography and magnetic resonance spectroscopy (MRS) to detect metabolism in cancer, a basic review of the physics of hyperpolarization, and a summary of recent applications in biology. Although many of the important recent advances are technical, those have been de-emphasized. Imaging hyperpolarized inert molecules such as those used for vascular imaging is also not discussed. Instead, we focus on tumor metabolism and the use of hyperpolarization methods to monitor dynamic metabolic processes *in vivo*. It should also be emphasized that other diseases—diabetes, ischemic heart disease, diffuse hepatocellular diseases, stroke, to name a few—are also associated with marked metabolic abnormalities and that new methods to probe tissue biochemistry should be equally valuable. The academic and industrial communities have an unusual opportunity and perhaps a responsibility to move this technology forward quickly because there is a strong clinical need to acquire quantitative information about metabolism in primary and metastatic lesions to enhance cancer care. Although it is true that hyperpolarized MR is technically challenging, the underlying MRI techniques and necessary engineering knowledge are currently available. Furthermore, the chemical principles and knowledge of biochemical pathways required to interpret the images are also well known. There are no known insurmountable barriers in developing this technology for human studies, and a future role in assessment of cancer patients can be envisioned.

Metabolism in Cancer

Cancer metabolism can be viewed as the sum of a large but finite number of interdependent biochemical pathways, each of which provides a specific function for the cell [1,2]. Many of these pathways, particularly glycolysis, the pentose phosphate pathway, the tricarboxylic acid (TCA) cycle, oxidative phosphorylation, and the synthesis of nucleotides and lipids, either are required to support the intense biosynthetic demands of cell proliferation or are subject to alternative regulation in cancer. Below, we outline six concepts that illustrate the important links between tumor biology and metabolism.

Historically, the first important concept was that tumor metabolism differs from that of the surrounding tissue. In the 1920s, Otto Warburg demonstrated that tumors had high rates of glucose consumption and lactate production compared with the normal tissue [3,4]. This seminal observation created the field of tumor metabolism, which has been dominated largely by the study of glycolysis ever since [5]. Enhanced fluxes in other pathways including lipid synthesis, amino acid transport, and nucleotide transport have also been observed in aggressive tumors and are being investigated for diagnostic purposes [6] or as therapeutic targets [7–9].

Regulation of tissue pH is also abnormal in cancer. Most tumors have an acidic extracellular pH compared with normal tissue, and this can be correlated with prognosis and response to treatment [10–12]. Secondary changes in malignant tissue such as inflammation and ischemia are among the pathologic states associated with an altered acid-base balance [13–16]. Despite the importance of pH and its relationship to the disease, there is currently no clinical tool available to image the spatial distribution of pH in humans.

More recently, it has been shown that tumor suppressors and oncogenes regulate nutrient uptake and metabolic flux. Thus, tumor metabolism is linked mechanistically to the mutations that cause cancer. As early as the 1980s, it was determined that overexpressing the oncogenes *ras* or *src* in fibroblasts was sufficient to drive glucose uptake [17], and numerous subsequent studies have documented the metabolic effects of various mutations or aberrant signaling activities. Many of these studies have focused on glucose uptake, but others suggest wider influence involving either the specific fates of glucose carbon within the cell or the ability to orchestrate multiple pathways simultaneously. For example, the oncogenic transcription factor c-Myc seems to regulate cellular handling of both glucose and glutamine, which, together, feed the metabolic pathways required for cell growth and

proliferation [18–20]. Deletion of the tumor suppressor gene *TP53* can stimulate glucose uptake and suppress the oxidation of pyruvate, both of which are hallmarks of the metabolic phenotype described by Warburg [16,21]. Together, these observations support the notion that alterations in metabolism are common downstream indicators of the transformed state.

A fourth and perhaps surprising principle is that mutations in metabolic enzymes may cause a small number of cancers. Pheochromocytoma and paraganglioma can be caused by mutations in subunits of succinate dehydrogenase, an enzyme complex that [16,21] functions in both the TCA cycle and electron transport [13,22,23]. Similarly, mutations in the TCA cycle enzyme fumarate hydratase occur in a familial form of leiomyomatosis and renal cell cancer [13,22,23]. In both of these diseases, affected patients inherit one mutant allele and their tumors exhibit loss of the other, resulting in a severe deficiency of enzyme activity in the tumor. The mechanism for tumorigenesis in these diseases is unknown but may be mediated by accumulations of succinate and fumarate, both of which have been demonstrated to elicit effects normally brought on by hypoxia [24]. More recently, mutations in the two isoforms of isocitrate dehydrogenase, IDH1 and IDH2, were identified in glioblastoma, low-grade gliomas, and acute myelogenous leukemia [25–27]. Although the mutant enzymes lack the canonical IDH enzymatic activity, the genetics of these tumors pointed to a more complex mechanism of tumorigenesis than simple loss of function. In particular, the fact that these somatically acquired mutations were confined to a single codon and were not accompanied by loss of heterozygosity suggested that the mutant alleles functioned as oncogenes. Consistent with this idea, mutant IDH1 proteins were recently shown to possess a new enzymatic activity, the production of the metabolite 2-hydroxyglutaric acid from alpha-KG [28]. It should be noted that several other inborn errors of metabolism, including glycogen storage disease type 1 and tyrosinemia type 1, are also associated with cancer. These findings together indicate that the detection of abnormal metabolic fluxes or the accumulation of unusual metabolites could be used to monitor the predisposition to cancer in humans.

Some aspects of metabolism may predict disease severity or outcomes in cancer. For example, the enzyme transketolase-like 1 (TKTL1), which catalyzes transfer reactions between glycolysis and the nonoxidative branch of the pentose phosphate pathway, is overexpressed in a number of tumor types. A large study involving more than 1000 primary tumor samples determined that a high expression of TKTL1 predicted early mortality in colon and urothelial cancers [29]. Another study demonstrated a similar connection between TKTL1 expression and distant metastases in ovarian carcinoma [30]. These observations raise the appealing possibility that methods to monitor the activity of TKTL1, fatty acid synthase (FAS), and other enzymes *in vivo* would provide novel biomarkers of disease severity, enabling clinicians to tailor treatment regimens.

Finally, clinical oncologists have long known that tumor growth can be suppressed by modifying metabolic activity in some instances. For example, L-asparaginase, an important component of treatment regimens in pediatric leukemias, operates on the principle that the demand for asparagine in rapidly proliferating tumor cells exceeds what can be supplied through endogenous *de novo* asparagine synthesis. Infusion of L-asparaginase reduces the availability of asparagine from the blood supply, thereby specifically limiting the growth of the tumor cells. Antimetabolite therapies such as methotrexate suppress *de novo* nucleotide synthesis in proliferating cells. More recent studies have demonstrated that genetic or pharmacological manipulations of other metabolic activities are effective in limiting the growth of xenografts [31–34]. These studies have generated excitement about developing related approaches in human cancer.

Role of Molecular Imaging in Clinical Oncology

Tissue biopsy and histopathology at a single point in time is the standard approach to diagnose cancer. Once a diagnosis is established, therapeutic decisions and follow-up typically rely on a combination of clinical evaluation and radiologic imaging. Of course, methods that require invasive tissue sampling are undesirable in many respects, particularly for longitudinal monitoring, screening programs, and efforts to understand factors influencing cancer risk. For these reasons, there is intense interest in minimally invasive technologies that provide specific diagnoses, information about the disease stage, and prediction and/or assessment of response to therapy.

Molecular imaging may be defined as "the visualization, characterization, and measurement of biologic processes at the molecular and cellular levels" [35]. In principle, molecular imaging methods can detect specific biologic processes that are changed in cancer relative to surrounding normal tissue. The power of molecular imaging lies in the fact that it is essentially noninvasive and thus can be used to probe the whole tumor volume repeatedly over time. Imaging can not only support an initial diagnosis but also monitor progress in terms of staging, restaging, treatment response, and identification of recurrence, both at the primary tumor and at distant metastatic sites. For the purposes of this report, we consider "metabolic imaging" as a subset of molecular imaging methods that provide more-or-less direct information about tissue metabolism. Many research methods are sensitive to tissue metabolism, but we limit our comments to two metabolic imaging methods that are widely used in clinical practice or clinical research: positron tomography and MRS.

Positron Emission Tomography

Positron emission tomography (PET) images the uptake of an injected radiolabeled molecule in the tumor and, when combined with x-ray computed tomography (CT), provides both molecular information and anatomic localization. The amount of radiolabeled material that is injected is negligible compared with the normal concentration of metabolites, and consequently, PET tracers do not disrupt tissue physiology. The most commonly used PET tracer is [^{18}F]-fluoro-2-deoxyglucose (FDG), which exploits the high glycolytic rate of many tumors. Because of high levels of glucose transporters and hexokinase activity, cancer cells demonstrate high FDG uptake and phosphorylation compared with the normal tissue. Phosphorylated FDG cannot be metabolized further and becomes "trapped" inside the tumor, and over time, regions of high FDG accumulation can be easily distinguished. The diagnostic power of FDG-PET lies in its ability to stage disease, monitor treatment response, and detect recurrence, rather than in initial diagnosis [36].

Many other clinically relevant features of tumor metabolism can be probed with current PET technology. For example, choline, which is transported into cells and incorporated into phospholipids, can be labeled with either [^{11}C] or [^{18}F] and has found application primarily in prostate cancer [37,38], hepatocellular carcinoma [39], and lung and brain lesions [40]. Cell division has been monitored with the thymidine analog, 3′-deoxy-3′-[^{18}F]fluorothymidine. It is trapped in cells after phosphorylation by thymidine kinase 1, which is especially active during the S phase of the cell cycle, and thus has been used to detect dividing cells *in vivo*. The diagnostic power of 3′-deoxy-3′-[^{18}F]

fluorothymidine is in distinguishing malignant from benign lesions, in assessing response to therapy, and in grading lung, breast, and colorectal cancers and lymphoma [41].

Other avenues of investigation in PET-based molecular imaging of cancer include the use of the somatostatin analog ^{68}Ga-DOTATOC, which binds to somatostatin receptor 2 with high affinity and has been used to diagnose neuroendocrine tumors [42]. Estrogen receptor (ER) expression can be imaged using 16-α-[^{18}F] fluoro-17-β-estradiol, which binds to both subtypes ERα and ERβ. Arginine-glycine-aspartic acid–containing peptide ligands, which bind to the $\alpha_v\beta_3$ integrin that is upregulated on angiogenic blood vessels, have shown promise for imaging tumor angiogenesis and assessing the effects of antiangiogenic drugs [43]. Hypoxia, resulting from an imbalance between perfusion and metabolism, can be imaged by exploiting the reduction and binding of nitroimidazoles under hypoxic conditions [44].

These and other PET agents have been used extensively in clinical oncology research, and their practical value in the clinic has been demonstrated. However, the value of these techniques for determining the fate of a tracer in alternative metabolic pathways is limited by the absence of chemical information in PET images. Inevitably, there are also concerns related to radiation dose with PET/CT and the practicalities of radiation containment in the clinic.

MRI and MRS

^{1}H MRS can easily be incorporated into existing MRI examinations [45–47] using currently available clinical MR scanners. For these reasons, there has long been interest in evaluating endogenous tumor metabolites by ^{1}H MRS owing to its relatively high sensitivity and nearly 100% natural abundance.

^{1}H signals from choline-containing molecules are frequently elevated in cancer, and this has been correlated with cellular proliferation in brain, prostate, breast [46,48,49], colon, and cervical cancers [50]. Choline abundance can be used to predict the tumor's histologic grade with low false-positive and false-negative rates. For example, many breast tumors show high concentrations of total choline [51,52], whereas benign lesions are generally contain low concentrations of choline [53]. Moreover, spatial mapping of choline signals can reveal aggressive tumor regions and their response to therapy [50]. Because brain tumors exhibit elevated choline and decreased *N*-acetyl aspartate concentrations, the Cho/*N*-acetyl aspartate ratio has been widely used as a prognostic marker to distinguish low- and high-grade disease in astrocytomas [54,55] and gliomas [56]. Monitoring the increase in this ratio may also be useful for detecting progression [56]. Other metabolite ratios, such as choline/creatine, can differentiate low-grade glioma from benign demyelinating disease [57] and high- from low-grade oligodendroglial tumors [58]. Prostate ^{1}H spectra exhibit elevated choline and reduced citrate in regions of prostate cancer [46].

The relatively poor spatial resolution in MRS imaging (MRSI), typically resulting in voxels of 0.16 to 1 cm^3 [46,49,59,60], is a limiting factor. Nonetheless, if validated in large-scale trials, MRS could improve clinical characterization of brain lesions and potentially avoid difficult biopsies. Breast MRS could be a valuable adjunct to MRI for lesion grading and monitoring of treatment response, particularly for improving specificity. Prostate cancer localization and grading through three-dimensional MRSI could be used to select patient groups in which biopsy is not necessary, saving patients unnecessary invasive procedures and anxiety. MR, of course, offers the opportunity to detect drugs and other metabolism by ^{19}F [61,62], ^{31}P [63,64], and ^{13}C [65], but these research applications are not widespread. In the future, large-scale, multisite, prospective trials are needed to confirm the very promising results of ^{1}H MRS achieved thus far to assess clinical value.

Current Limitations of Molecular Imaging

Many clinically relevant aspects of tumor cell biology are reflected in metabolic activity. Moreover, the complexity of intermediary metabolism also provides a host of potential targets to image. Unfortunately, current modalities provide only snapshots of metabolism and are blind to many of the subtleties that reflect the tumor's biologic state. For example, despite FDG-PET's success in detecting tumors [5], not all tumors consume glucose avidly enough to give a positive FDG-PET signal. A "cold" tumor could be metabolically inactive, or it might use alternative substrates to support survival and to fuel growth. A more vexing problem is that even a positive result on FDG-PET is open to multiple interpretations because FDG-PET provides no information about glucose metabolism beyond import and phosphorylation. Carbon from glucose can supply glycolysis, the pentose phosphate pathway, oxidative metabolism in the mitochondria, and biosynthetic reactions, each of which serves different functions within the cell. The allocation of carbon from glucose and other nutrients into these pathways is determined by a combination of extrinsic and intrinsic modifiers of metabolism and ultimately determines whether tumor cells die or survive and whether they remain quiescent or undergo growth and proliferation [1]. For example, glucose uptake is stimulated by the activation of oncogenic signaling [17,66] or by hypoxia, which suppresses the entry of glucose carbon into oxidative pathways and inhibits proliferation [67]. Thus, it is impossible based on FDG-PET alone to know whether a tumor is growing actively.

^{1}H MRS is attractive but with most clinical systems, only a limited number of metabolites are present at concentrations that allow useful spatial mapping. This significantly limits the level of analysis possible for a tumor. The information is in some ways more useful than PET in that multiple metabolites can be spatially resolved in a single imaging protocol. However, only static concentrations are detected, rather than tracer uptake, which is one of the most useful features of FDG-PET.

What Is Hyperpolarization?

It is convenient to think of MR as a process to detect alignment of magnetic nuclei with or against an applied magnetic field. The term *polarization* refers to the difference in the fraction of nuclei in these two energy states. Under normal conditions, the degree of nuclear spin polarization is proportional to the gamma (γ) and B_0/T, where γ is the nucleus-specific gyromagnetic ratio constant, B_0 is the applied magnetic field, and T is the temperature in Kelvin. The MR signal is proportional to the spin polarization that is typically on the order of 0.0001% to 0.0005% depending on the nucleus and field. This very low level of polarization results in one of the main drawbacks of all MR methods, namely, limited signal. In fact, clinical MRI is so successful only because the high concentration of protons in water and fat overcomes poor polarization. Efforts to improve signal by increasing the applied field B_0 are feasible but limited to only a few folds by practical constraints and cost.

In the context of MR, the term *hyperpolarization* refers to a procedure that drives nuclei, temporarily, into a significant redistribution of the ordinary population of energy levels. This artificially created nonequilibrium condition of the nuclei in a magnetic field can be accomplished using various techniques as described in recent review

articles and book chapters [65,68–71]. On hyperpolarization, the signal from a given number of nuclear spins can be raised by a factor of 10,000 or more when compared with equilibrium conditions in clinically available MRI scanners. This staggering increase in signal has the potential to substantially overcome one of the key limitations of MR: limited sensitivity.

Multiple methods, outlined below, have been described to generate the hyperpolarized state. Regardless of method, the hyperpolarized spin states are not stable in the sense that the induced massive spin polarization decays during a relatively short period to an equilibrium value. The rate of this exponential decay process is governed by spin-lattice relaxation with a time constant T_1. A slow relaxation rate corresponds to a long T_1. Because the ultimate goal of using hyperpolarization in biomedicine is to image metabolic events in real time, hyperpolarized states with sufficiently long lifetimes (>20 seconds) are required. Long T_1's are typical for relatively low-γ nuclei such as ^{13}C. The relaxation rates are generally longer than those of protons. Carbon nuclei that are not directly bonded to protons such as carboxyl carbons or quaternary carbons have T_1's ranging up to 80 seconds depending on the molecule and the magnitude of B_0.

The first and still the only hyperpolarization method that has been used to generate polarized materials for human studies is optical pumping of ^3He or spin-exchange optical pumping of ^3He and ^{129}Xe [72–76]. Two other hyperpolarization techniques have been developed for applications to MRS and MRI: parahydrogen-induced polarization (PHIP) [77,78] and dynamic nuclear polarization (DNP) [79,80]. Both methods can be used to polarize molecules containing ^{13}C, an important advance because of the very large chemical shift range of ^{13}C in organic molecules and the opportunity for direct tracing of drugs or key metabolic intermediates.

Parahydrogen-Induced Polarization

PHIP methods exploit the spin order of the parahydrogen singlet state—the source of hyperpolarization. Although they can be implemented in a number of ways to use the spin order of parahydrogen singlet, the parahydrogen and synthesis allow dramatically enhanced nuclear alignment (PASADENA) effect is most widely used to prepare hyperpolarized tracer compounds [77,78,81]. PASADENA is unique in its ability to achieve hyperpolarization in aqueous medium in seconds, using *cis* addition of parahydrogen (pH_2) across alkene or alkyne bonds followed by the spin order transfer from nascent protons to ^{13}C or ^{15}N with a theoretical polarization limit of 100%. PASADENA is also inexpensive, portable, and easy to maintain, as the hyperpolarization can be conducted in a low-field magnet of only a few millitesla [82]. Rh-based molecular catalysts allow molecular hydrogenation of the unsaturated bond and spin order transfer from parahydrogen spins on the time scale of several seconds [82]. The toxicity of the catalyst remains a concern for extending PHIP to clinical applications.

The spin order transfer sequence used in PASADENA relies on the spin-spin couplings between the parahydrogen and the ^{13}C or ^{15}N nuclei of the labeled substrate. Deuteration of the hyperpolarized substrate is desirable in simplifying the spin system and in increasing the lifetime of the hyperpolarized substrate [83]. The development of metabolic imaging applications using the PASADENA technique is hampered by the requirement to have a precursor molecule that can be hydrogenated. This limits the choice of target molecules for imaging. Recently, an alternative PHIP method has been proposed under the acronym SABRE (signal amplification by reversible exchange) [84,85] in which the polarization transfer step does not require a hydrogenation reaction. Instead, the parahydrogen and target molecules are brought together temporarily on a suitable template, and the polarization is transferred in a low magnetic field from the hydrogen nuclei in the parahydrogen to scalar coupled nuclei (hydrogen and *X*-nuclei) in the target molecule. The polarization transfer process can generate *Z*-magnetization but also multiple spin coherences [86] and is therefore particularly suited for the generation of long-lived states [87–90]. Retaining the advantages of hydrogenative PHIP, this new method may allow the polarization of additional molecules.

Dynamic Nuclear Polarization

DNP is based on the transfer of polarization from the electron spins of paramagnetic centers embedded in a glassy frozen solution to neighboring nuclear spins through dipolar interactions [79,80]. Because the magnetogyric ratio of an electron is so high compared with that for any nucleus, at any applied field, unpaired electrons will be more polarized; the goal is to transfer this polarization to informative nuclei. For the technique to be efficient, the paramagnetic centers, usually stable radicals, have to be homogeneously distributed in the frozen solution containing the molecules of interest. The optimal temperature for an efficient polarization transfer is about 1 K. DNP methods were developed initially for applications in nuclear and particle physics research, but they became of interest for biomedical applications after the introduction of the dissolution method by Ardenkjaer-Larsen et al. in 2003 [80]. The dissolution step rapidly transforms the frozen solution into a dilute room temperature solution in which the nuclear spins of the molecules of interest remain polarized. The molecules are then considered to be hyperpolarized. Dissolution DNP yields ^{13}C nuclear polarization in liquids up to about 40% in selected molecules [80]. The technique is quite versatile and has been used to hyperpolarize ^1H, ^6Li, ^{13}C, ^{15}N, and ^{89}Y in a variety of molecules or nanoparticles [56,69,91–97].

The crucial ingredients for efficiently hyperpolarizing molecules through DNP are the following: 1) Efficient paramagnetic centers (stable free radicals); trityl radicals have been the most commonly used free radicals to date. 2) Adapted cryogenic equipment to keep the frozen solution at around 1 K during the microwave irradiation driving the polarization transfer; two designs have been implemented so far: a system with a variable temperature insert that is placed in the helium bath used to maintain the polarizer superconducting magnet at 4.2 K [96] and a system with a separate cryostat that can be inserted in a standard room temperature bore superconducting magnet [98]. In addition, although the original field used in dissolution DNP was 3.35 T, it has recently been shown that greater polarization can be obtained at higher fields, about 4.6 to 5.0 T [99,100]. 3) An efficient means is needed to dissolve the frozen solution and rapidly transfer it to the MR equipment with minimal loss of the hyperpolarized state; a specific device minimizing the delay between the dissolution and the infusion of DNP-enhanced molecules has been implemented for *in vivo* applications [98].

The applicability of this technique to investigating metabolic pathways requires that the ^{13}C or ^{15}N labeled substrate is a water-soluble, endogenous or exogenous metabolite with a long T_1 relaxation time in the liquid state. A limitation that still has to be overcome is the relatively long period required to prepare the hyperpolarized nuclei, typically 30 to 90 minutes, when using DNP. The strength of DNP is that, in principle, virtually any biomolecule can be hyperpolarized. However, in practice, the ability to capitalize on the potential of new

hyperpolarized probes requires knowledge of whether the probe polarizes sufficiently, which is an interplay between spin diffusion, polarization transfer, and relaxation.

Nuclei for Hyperpolarization and the Role of Relaxation

As we have seen, multiple methods can induce a hyperpolarized state. However, once the hyperpolarized compound is delivered *in vivo*, the hyperpolarized state decreases to its equilibrium value with a time constant according to the spin lattice relaxation time T_1. As a result of both metabolism and this relaxation process, the resulting MR signal can be significantly reduced when detected *in vivo*. Consequently, a critical challenge in translation of this technology is development of probes that balance three features. First, the T_1 must be sufficiently long so that a significant fraction of the hyperpolarized state is preserved *in vivo*. Second, the metabolic pathway or process must be sufficiently rapid that, given the T_1 of the polarized molecule, useful information can be obtained. Third, the process or pathway must be relevant to tumor biology.

These factors are also relevant, of course, in design of agents for positron tomography. In other respects, studies with hyperpolarized ^{13}C or ^{15}N are quite different. For example, the half-lives ($t_{1/2}$) of tracers used typically in PET such as ^{11}C or ^{18}F (20 or 110 minutes, respectively) are often much longer than polarized states achieved so far, which often decay with relaxation times on the order of only 20 to 60 seconds. This problem is partially alleviated because, unlike with nuclear medicine probes, there is no need to wait for clearance of hyperpolarized probes before imaging; in fact, one images immediately after the administration of the probe providing information on uptake, biodistribution, and metabolism of the probe in a scan time of a minute or less. This has several advantages such as the ability to image metabolism in a breath hold, observe fast metabolic fluxes (i.e., the conversion of pyruvate to lactate by lactate dehydrogenase [LDH]), and the ability to add a hyperpolarized metabolic imaging scan to an MR clinical scan without significant time penalty. Nonetheless, the short lifetimes significantly restrict the generality of hyperpolarized MR for *in vivo* imaging.

PET nuclei have exact $t_{1/2}$ values that are insensitive to their chemical environment. T_1 relaxation times are dependent on the nucleus but are also sensitive to a host of other factors including the applied field, the location in a molecule, molecular structure and motion, and the chemical environment. Despite this complexity, some generalizations can be made. Hydrogen nuclei, because of their large γ values, interact more strongly with their surroundings and thus have relaxation times of a few seconds or less. Thus, whereas water protons have been polarized using DNP and this offers the interesting possibility of using water as a contrast agent, the short T_1 (2.7 seconds) is a limiting factor for its use *in vivo* [101]. In many circumstances, the polarization of ^{13}C and ^{15}N molecular sites will persist for much longer. The fundamental reason for the longer lifetimes of hyperpolarized ^{13}C and ^{15}N arises from their lower γ compared with that of protons. However, direct bonding to dipoles such as ^{1}H, of course, reduces the T_1's of ^{13}C and ^{15}N significantly. Although some ^{15}N-enriched hyperpolarized probes have longer T_1's compared with ^{13}C probes, there are significantly more carbon sites present in the metabolic probes of interest. As a result, ^{15}N use may be limited to a narrower range of probes such as hyperpolarized ^{15}N-choline [92].

Other nuclei that have been polarized using DNP include ^{6}Li and ^{89}Y. ^{89}Y is a spin half-nucleus that is difficult to detect at thermal polarization levels because of its small magnetic moment. However, its long T_1 ($\gg$100 seconds) makes it attractive as a DNP probe. ^{89}Y-labeled complexes have been polarized using DNP to levels of up to 1527-fold above thermal equilibrium at 310 K [102]. ^{6}Li also has a long T_1 (~120 seconds) and $^{6}LiCl$ has been polarized using DNP [95,102]; the decay of the hyperpolarized ^{6}Li signal is extremely sensitive to small quantities of MR contrast agents and can be used to enhance the sensitivity of detection of these agents. Provided that sufficient ^{6}Li distribution and detection can be achieved, the decay of the hyperpolarized ^{6}Li signal can then be used as a sensitive probe to detect trace quantities of MR relaxation agents.

Acquisition Techniques for Hyperpolarized ^{13}C Imaging

Imaging the metabolic products of hyperpolarized ^{13}C or other nuclei places special demands on the MR scanner, the pulse sequences, and data processing. The primary limitation arises from the T_1 relaxation times of the label in the parent molecule and its metabolic product(s) that causes the hyperpolarized signal to decay back to its thermal equilibrium. The amount of detectable signal available for imaging will be a function of the degree of polarization, the T_1 relaxation time, and the concentration of the metabolite. As a rough estimate, the available time for imaging with an initial signal enhancement of 10,000 is probably five to nine times the T_1 relaxation time. Also, each RF excitation, repeatedly applied during data acquisition, causes a loss of hyperpolarized signal, and thus, acquisitions minimizing the number of RF pulses are preferred. The optimum time window in which to record a maximum signal arising from the metabolic products after conversion will be a balance between systemic delivery of the hyperpolarized compound and the rate of conversion to its downstream metabolic products in the tissue/tumor region of interest.

Owing to the nonrenewable nature of the magnetization and fast decay, signal sampling needs to minimize the acquisition time, minimize the number of excitation pulses, and maximize the retention of polarized signal. How this is best achieved depends on the nature of the measurement, on the T_1 relaxation time, and on the dynamics of the process under observation. A variety of acquisition strategies have been developed to maximize the signal-to-noise ratio (SNR) and resolution while minimizing the number of excitations [103,104]. For slice or coil-only localized spectroscopy, commonly a short repetition time (compared with T_1) and a small flip angle pulse and acquire sequence has been used [105,106].

If only a single resonance is to be measured, and any other spectral lines can be excluded by for example, selective excitation, imaging techniques developed for evaluation of hyperpolarized gases He and Xe can be used [107]. Many studies have made use of small-tip angle pulse sequences [80,105,108–112]. A variable flip angle technique can maximize sampling of the available polarization while ensuring that signal at each acquisition remains approximately constant [113] rather than progressively declining as would be the case with a constant flip angle acquisition. To optimize this approach, the T_1 relaxation time(s) *in vivo* must be known, and the flip angle needs to be accurately calibrated.

As the hyperpolarized magnetization decreases toward equilibrium, the metabolic conversion of the substrate occurs rapidly, sometimes in just a few seconds. Hence, for metabolic imaging, the desired information lies in both the spectral domain, with the relative amplitudes of the different chemical shift species, and the spatial and temporal domains. This necessitates spectral encoding along with the rapid acquisition of imaging data, which strongly influences the design of

pulse sequences for this application. Several fast spectroscopic imaging approaches that provide spatial and spectral information on the uptake and metabolism of hyperpolarized probes have been used [113–115]. Single-slice two-dimensional spectroscopic imaging with elliptical central *k*-space sampling has provided both spatial and spectral information in a rapid acquisition for preclinical cardiac measurements [115]. A three-dimensional volume sampling approach using phase encoding in two spatial dimensions and an echo-planar readout gradient in the third dimension has been widely used for 15-second ^{13}C spectroscopic imaging [113,114]. To improve acquisition time and efficiency for practical clinical application, data acquisition accelerations achieved by reducing the number of temporal samples and using advanced reconstruction methods to recover the missing information are being explored. These include using a least squares approach and prior knowledge about the spectral components [111], randomly distributed samples, and a reconstruction based on L1 minimization (compressed sensing) [103,116] and parallel signal reception [117].

Special excitation pulses have been used to reduce sampling of the initially polarized substrate, thus leaving more polarization available for detection as newly synthesized metabolites [118,119]. Pulses with a spectral response consisting of multiple bands have been used [120,121], with a smaller tip-angle band applied to the frequency of the substrate and a larger tip-angle band applied to the frequencies of the products. This approach has improved the SNR of the products by preserving the polarization of the substrate and allowed serial spectroscopic imaging with a time resolution of 3 seconds to monitor the temporal dynamics of ^{13}C-pyruvate uptake and metabolism [120].

Physiology and Metabolism in Preclinical Models

A major challenge facing hyperpolarized MR is the relatively short duration of polarization. This means that, to study metabolism, the substrate must be rapidly transported through the bloodstream to the tissue of interest, be rapidly taken up by the cell, and be rapidly metabolized. Furthermore (unlike PET tracers), the mass of the substrate that must be injected is substantial and sufficient to alter metabolic processes. If that substrate is to be used in the clinic then it must be nontoxic at the relatively high concentrations. Alternative substrates may be developed, but even if the substrates that have been used successfully so far are the only ones to make it to the clinic, it is already clear that these could provide unique and important information on tumor grade, prognosis, and treatment response. In discussing the potential of hyperpolarized substrates for imaging cellular metabolism in cancer and other diseases, perhaps the best approach is to discuss the substrates or probes that have been successfully hyperpolarized and to describe how they have been used in preclinical models and their clinical potential.

Metabolism of Hyperpolarized Pyruvate

[1-^{13}C]Pyruvate has been the most widely studied substrate to date, reflecting its central role in cellular metabolism, the ease with which it can be hyperpolarized, its relatively long T_1 relaxation time, and its very rapid transport across the cell membrane and subsequent metabolism. High solubility in water is also a factor because it means that the concentration of the hyperpolarized material is still relatively high after dissolution. Pyruvate, the end product of glycolysis, can be reduced by the NADH produced in the pathway to generate lactate, in the reaction catalyzed by the enzyme LDH. Alternatively, pyruvate undergoes transamination with glutamate to form alanine, in the reaction catalyzed by alanine transaminase (ALT). The reactions catalyzed by both LDH and ALT are readily reversible in the cell and therefore the polarized ^{13}C label introduced in [1-^{13}C]pyruvate can effectively exchange with preexisting pools of lactate and alanine [122]. A third reaction involves the irreversible decarboxylation of [1-^{13}C]pyruvate to hyperpolarized ^{13}C-labeled carbon dioxide in the reaction catalyzed by the mitochondrial enzyme, pyruvate dehydrogenase (PDH). The carbon dioxide released is subsequently interconverted with bicarbonate in the reaction catalyzed by carbonic anhydrase. The reactions catalyzed by LDH and ALT have been observed to be altered in cancer [110,123–126] as is the monocarboxylate transporter that mediates pyruvate uptake and lactate export [127]. All three reactions have been observed in normal and pathologic cardiac tissue [115,128–130].

MR observation of hyperpolarized products of pyruvate metabolism can be performed with very high temporal resolution, up to one measurement per second (Figure 1). The practicality of these kinetic measurements opens the possibility that direct measurements of absolute fluxes may be feasible *in vivo* at some point in the future. It is important to emphasize that, as a consequence of the inherent chemical information in the ^{13}C NMR spectrum, the ability to detect metabolism of a labeled molecule through a single enzyme-catalyzed reaction *in vivo* is already a reality (Figure 1).

[1-^{13}C]pyruvate: Applications to Cancer

In a murine lymphoma model, the LDH-catalyzed interconversion of hyperpolarized label between pyruvate and lactate was shown to decrease early after chemotherapy [124]. Transfer of this technique to the clinic may allow an oncologist to determine whether a cancer is responding to the treatment within hours of treatment. If the tumor is not responding, a more effective treatment regimen could be initiated; rapidly changing the patient to a more effective drug not only is cost-effective but also can greatly improve morbidity and mortality [71]. The decreased LDH-catalyzed flux in this study was explained by a loss of the coenzyme NAD(H), decreases in tumor cellularity, and reduced LDH concentrations. Another study compared the treatment response detected with hyperpolarized pyruvate with that detected from measurements of FDG uptake [131]. A decrease in FDG uptake was found to precede the decrease in flux between pyruvate and lactate. However, by 24 hours after drug treatment, the magnitude of both the decrease in FDG uptake and the decrease in pyruvate to lactate flux was comparable.

Flux of hyperpolarized ^{13}C label between pyruvate and lactate has also been used as a marker of prostate cancer progression, with the levels of hyperpolarized lactate increasing with increasing tumor grade in the TRAMP model [123] (Figure 2). Determining tumor grade in the clinic is normally limited by sampling problems during biopsy, but transfer of this method to the clinic could allow noninvasive determination of the whole prostate. Another report has demonstrated significantly higher hyperpolarized lactate production in two human glioblastoma xenograft models, where the blood-brain barrier has been disrupted, relative to normal brain, suggesting that hyperpolarized MR metabolic imaging may be valuable for assessing prognosis and monitoring response to therapy for patients with brain tumors [125]. Tumor oxygenation status is also a key determinant in both tumor growth and response to therapeutic interventions, particularly radiation-based therapies. Combined hyperpolarized MRI of [1-^{13}C]pyruvate with electron paramagnetic resonance imaging of the trityl radical, used in hyperpolarization, has allowed the acquisition of images of hyperpolarized lactate coregistered with P_{O_2} maps in a murine tumor model [132].

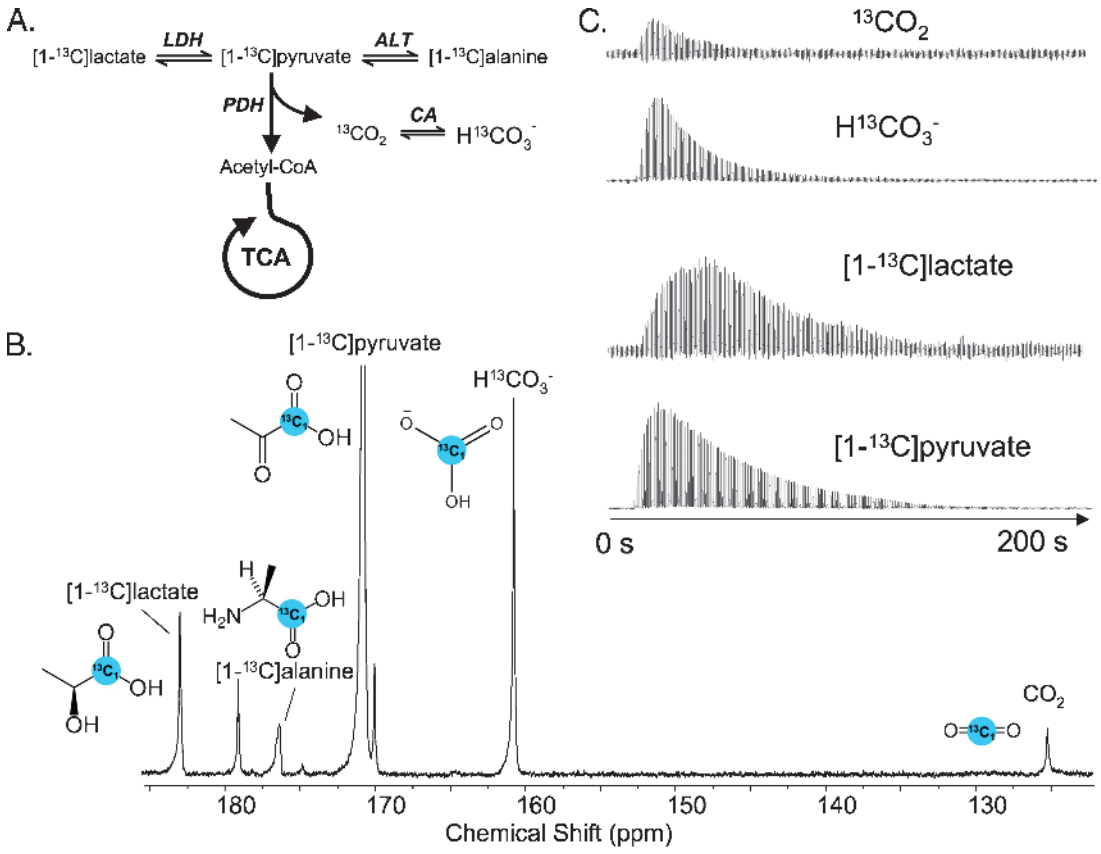

Figure 1. (A) Diagram demonstrating the metabolism of [1-^{13}C]pyruvate, which can be converted to [1-^{13}C]lactate in a reaction catalyzed by the enzyme LDH, [1-^{13}C]alanine in a reaction catalyzed by ALT, and ^{13}C-carbon dioxide in a reaction catalyzed by PDH). The carbon dioxide released is subsequently interconverted with bicarbonate in a reaction catalyzed by carbonic anhydrase (CA). (B) The great strength of hyperpolarized ^{13}C NMR is the ability to measure not only the uptake of the labeled substrate but also its metabolic products. For example, in the hyperpolarized ^{13}C NMR spectrum of an isolated rat heart perfused with hyperpolarized [1-^{13}C]pyruvate, metabolite resonances due to $^{13}CO_2$, $H^{13}CO_3$ [1-^{13}C]pyruvate, [1-^{13}C]lactate, and [1-^{13}C]alanine can be readily observed in a single acquisition. (C) Because of the dramatic increase in sensitivity of hyperpolarized MR, hyperpolarized products of pyruvate metabolism can also be measured with a 1-second temporal resolution and metabolic fluxes calculated from the kinetic information. Figure adapted from Merritt et al. [128].

Numerous mechanism-based anticancer drugs that target oncogenic signaling are in clinical trials. However, because such treatments can lead to tumor stasis, it remains challenging to assess responses by traditional imaging methods. In a recent study, inhibition through the phosphatidylinositol 3-kinase (PI3K/Akt/mTOR) pathway was shown to correlate with a drop in hyperpolarized [1-^{13}C]lactate levels in breast cancer and glioblastoma cells and xenografts [126]. The reduced appearance of lactate compared with pyruvate was attributed to a drop in LDH expression as a result of reduced levels of the transcription factor, hypoxia-inducible factor 1α, which regulates expression of the LDH gene [126]. These findings highlight the value of this technique as a method to confirm drug delivery and drug target modulation before, or in the absence of, apoptosis and a reduction in tumor size. An alternative to the lactate-pyruvate ratio, which is critically dependent on the timing of injection and subsequent data acquisition, is to measure the lactate and pyruvate signals over time and fit these to a kinetic model [124,126,133,134]. The fast spectroscopic imaging techniques described can also provide spatially resolved dynamic data of hyperpolarized pyruvate metabolism and spatially variable uptake of pyruvate, and the pyruvate-to-lactate flux observed in transgenic prostate tumors was consistent with tumor cellularity and necrosis [120].

Although the focus of this article is on the application of hyperpolarized [1-^{13}C]pyruvate to cancer, preclinical studies have demonstrated significant potential for studying both normal tissues and other human diseases. Hyperpolarized [1-^{13}C]pyruvate metabolism has been measured both *in vivo* and in the isolated perfused rat heart [115,128–130]. Metabolites identified include [1-^{13}C]lactate, [1-^{13}C]alanine, and $^{13}CO_2$. The latter was visualized through the production of ^{13}C-labeled bicarbonate ($H^{13}CO_3^-$) arising from the reaction catalyzed by PDH [128] (Figure 1). Fasted animals showed a reduction in hyperpolarized $^{13}CO_2$ production compared with fed controls, and a similar reduction was observed after the induction of type 1 diabetes, where the decrease correlated with disease severity [106]. Total global ischemia in isolated perfused rat hearts resulted in the production of [1-^{13}C]lactate and [1-^{13}C]alanine but not $H^{13}CO_3^-$ or $^{13}CO_2$ [129]. When [2-^{13}C]pyruvate was used instead of [1-^{13}C]pyruvate [130], the ^{13}C-label incorporated into citric acid cycle intermediates rather than being released as $^{13}CO_2$. In the perfused rat heart, the conversion of pyruvate to lactate, acetyl-carnitine, citrate, and glutamate was observed. The appearance of glutamate was slightly later than the other metabolites demonstrating flux through the citric acid cycle. After ischemia, citrate and glutamate decreased and lactate increased.

Detection of hyperpolarized pyruvate and its metabolic products has also been demonstrated in liver [135], muscle, and kidney [105,110]. One study demonstrated significant differences in the lactate-to-alanine ratio between the normal and fasted rat liver [135] and demonstrated a highly elevated hyperpolarized lactate in liver cancer [116].

There has been some debate as to whether pyruvate crosses the blood-brain barrier rapidly enough to allow imaging within the lifetime of the polarization. A recent study demonstrated detectable cerebral hyperpolarized [1-^{13}C]pyruvate metabolism; however, the lipophilic ethyl ester of pyruvate, ethyl pyruvate, was taken up and metabolized to a higher degree [136]. This study demonstrated that high doses of either hyperpolarized [1-^{13}C]-pyruvate or ethylpyruvate may be viable agents for brain imaging even in diseases that do not substantially affect the blood-brain barrier, for example, infiltrating gliomas, Alzheimer disease, nonenhancing multiple sclerosis, and acute stroke.

^{13}C-Enriched Bicarbonate

Extracellular pH has been measured in tumors by injecting hyperpolarized $H^{13}CO_3^-$ [137]. Measurements of the $H^{13}CO_3^-/^{13}CO_2$ ratio can be used to estimate the pH ($pH = pK_a + \log_{10}([H^{13}CO_3^-] / [^{13}CO_2])$) (Figure 3). The technique is ratiometric, so it does not require a measurement of absolute concentration, and the ratio changes by a factor of 10 in the physiological pH range. The rapid interconversion of $H^{13}CO_3$ and $^{13}CO_2$, catalyzed by carbonic anhydrase, ensures that the polarization decays at a similar rate in both species. pH images were obtained by measuring the $H^{13}CO_3/^{13}CO_2$ ratio in each imaging voxel, which demonstrated that the extracellular pH in a lymphoma tumor was more acidic than that in the surrounding tissue [137]. If this technique can be applied in the clinic, then it could be used as a generic marker of disease given the wide range of pathologic states that are associated with an acidic extracellular environment. Bicarbonate is

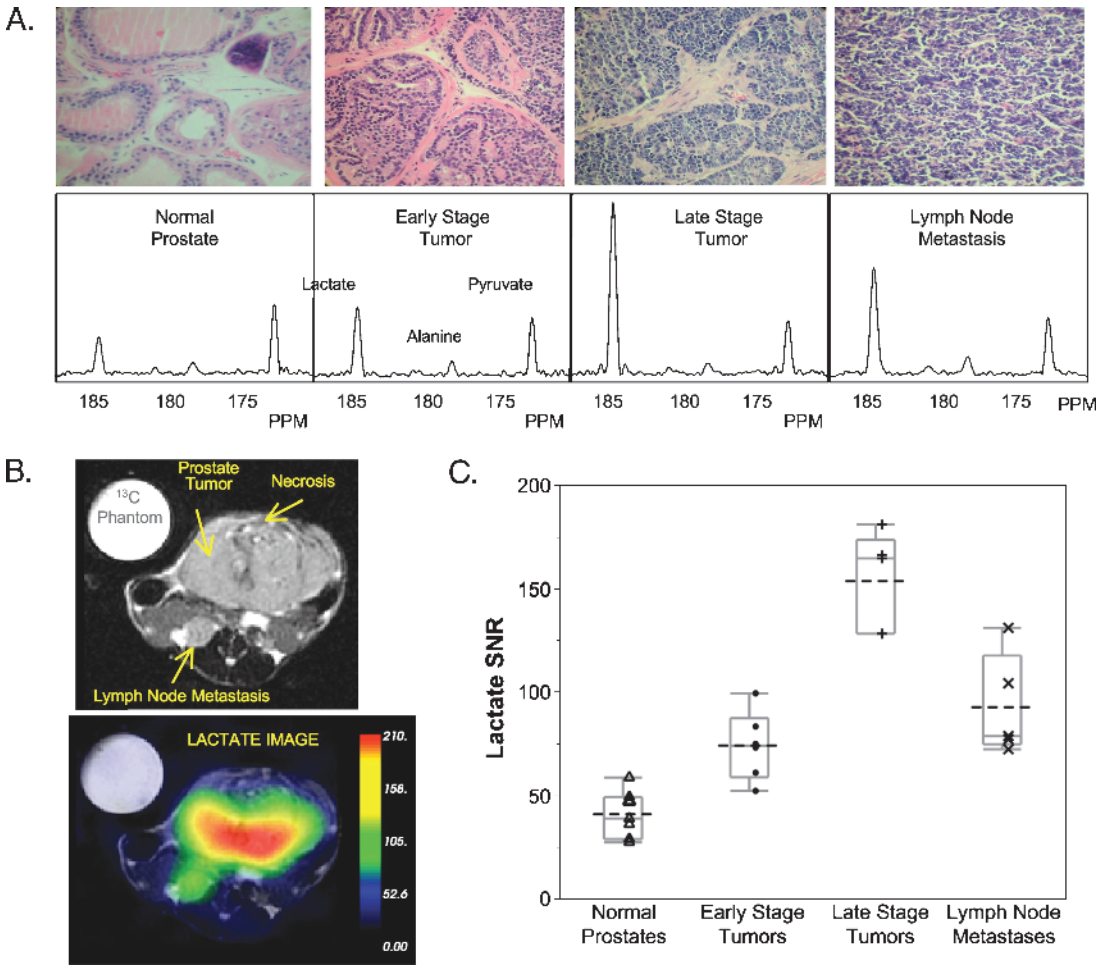

Figure 2. (A) Representative hematoxylin and eosin–stained pathologic sections (magnification, ×40) and hyperpolarized ^{13}C spectra from a normal mouse prostate, an early stage and late transgenic mouse prostate tumor (TRAMP), and a lymph node metastases. Below the histologic sections are representative hyperpolarized ^{13}C spectra acquired after injection of hyperpolarized [1-^{13}C]pyruvate and normalized to correct for differences in polarization. The normalized spectra exhibited a visually clear increase of hyperpolarized lactate and hyperpolarized lactate-to-pyruvate ratio with progression from the normal to early and late-stage tumors and metastases. (B) Axial T_2-weighted ^{1}H image depicting the primary tumor and lymph node metastasis from a TRAMP mouse with a late-stage primary tumor and the overlay of hyperpolarized [1-^{13}C]lactate image after the injection of 350 μl of hyperpolarized [1-^{13}C]pyruvate. Hyperpolarized [1-^{13}C] lactate increased in going from normal to prostate cancer and with disease progression. (C) A box plot quantitatively summarizing the peak area-to-noise ratios of the [1-^{13}C]lactate-to-noise ratio for the four histologically defined groups. The lactate peak area SNR values were statistically different ($P < .05$) for all four groups, except that early stage tumors were not significantly different from lymph node metastases. In addition, there was minimal overlap between individual [1-^{13}C]lactate-to-noise ratios between normal prostates and early and late-stage tumors. Figure adapted from Albers et al. [123].

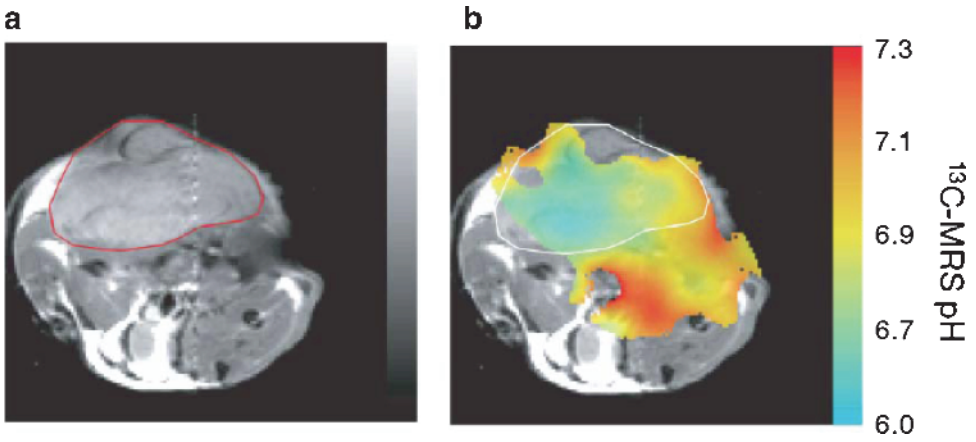

Figure 3. (A) Transverse proton MR image of a mouse with a subcutaneously implanted EL4 tumor (outlined in red). (B) pH map of the same animal calculated from the ratio of the $H^{13}CO_3$ acquired 10 seconds after intravenous injection of 100 mM hyperpolarized $H^{13}CO_3^-$ and assuming a pK_a of 6.17 ($pH = pK_a + \log([HCO_3] / [CO_2])$). Figure adapted from Gallagher et al. [137].

abundant in tissue (~25 mM) and is already infused into patients at concentrations that would be needed for a hyperpolarized ^{13}C imaging measurement of tissue pH.

[1,4-$^{13}C_2$]fumarate

After intravenous injection of hyperpolarized [1,4-$^{13}C_2$]fumarate, its metabolism to hyperpolarized [1,4-$^{13}C_2$]malate, catalyzed by the enzyme fumarase, has been demonstrated in tumors and skeletal muscle [138]. The signal from hyperpolarized malate increased significantly in skeletal muscle after ischemia and reperfusion [138], suggesting that it may be used as a positive contrast agent for identifying ischemic injury. The accumulation of malate was suggested to be due to a block in the TCA cycle [138]. However, recent studies in drug-treated tumors have demonstrated that the accumulation of malate is due to cellular necrosis [139]. In viable cells, the transport rate of fumarate into the mitochondria is too slow to enable the observation of labeled malate within the lifetime of the polarization. However, if this permeability barrier is removed, as it is in necrotic cells, then fumarate conversion to malate can be observed. Fumarate is potentially a useful agent for detecting treatment response in tumors because the production of labeled malate would seem to be an unequivocal indicator of cell death.

[1-^{13}C]lactate

[1-^{13}C]Lactate has been hyperpolarized and investigated as an *in vivo* metabolic imaging agent [140]. After intravenous injection in the TRAMP model, only low levels of hyperpolarized [1-^{13}C]pyruvate were detected, and this presumably reflects the exchange of label into a relatively small pool of tissue pyruvate. The hyperpolarized ^{13}C label was also diluted by flux into other metabolites, including [1-^{13}C]alanine and $H^{13}CO_3^-$. An important advantage of using lactate to introduce the hyperpolarized ^{13}C label is that the concentration of hyperpolarized lactate in the blood after injection is similar to that seen in an exercising animal; this differentiates it from hyperpolarized pyruvate, which is injected at a concentration that is much higher than is found endogenously.

[5-^{13}C]glutamine

Glutamine is important for tumor growth, and in many cell lines, its utilization is positively correlated with cell proliferation. Imaging glutamine metabolism could, therefore, be a marker of tumor growth and division and is already safely administered to humans in the clinic. The conversion of hyperpolarized [5-^{13}C]glutamine to [5-^{13}C]glutamate, catalyzed by intramitochondrial glutaminase, has been demonstrated in hepatocellular carcinoma cells *in vitro* [141]. The label in the C-5 position shows a larger chemical shift after conversion to glutamate compared with the C-1 position, which aids detection of the metabolite, although the T_1 is slightly shorter. The relatively low levels of polarization obtained in this study precluded studies *in vivo*. However, with higher levels of polarization, it may be possible to use this substrate to assess the effects of tumor treatment with cytostatic drugs.

[1-^{13}C]acetate

After injection of hyperpolarized [1-^{13}C]acetate into mice, both acetyl CoA and acetyl carnitine were observed in liver and heart, although the acetyl carnitine signal from the heart was higher, demonstrating an organ variation in the distribution of acetate metabolism [142]. Ischemia in skeletal muscle was shown to result in a reduction in acetyl-carnitine formation [142]. Carnitine can modulate fatty acid and carbohydrate metabolism by modifying the intramitochondrial acetyl-CoA/CoA ratio, and therefore, it is possible that this substrate could be used to probe fatty acid metabolism.

[2-^{13}C]-fructose

Owing to the limited lifetime of the hyperpolarized nucleus, with signal decay dependent on T_1 relaxation, carboxylate carbons have been the primary targets for development of hyperpolarized metabolic probes. The use of these carbon nuclei makes it difficult to investigate upstream glycolytic processes, which have been related to both cancer metabolism as well as other metabolic abnormalities, such as fatty liver disease and diabetes. Glucose carbons have short T_1's (<1 second) and therefore cannot be used as an *in vivo* hyperpolarized metabolic probe of glycolysis. However, the pentose analog fructose can also enter glycolysis through its phosphorylation by hexokinase and yield complementary information. The C2 of fructose is a hemiketal that has a relatively longer relaxation time (~16 seconds at 37°C) and high solution state polarization (~12%) [143]. Injection of hyperpolarized [2-^{13}C]-fructose into the TRAMP model demonstrated differences in uptake and metabolism in regions of prostate cancer relative to surrounding benign abdominal tissues [143].

[1-^{13}C]succinate

Succinic acid has been hyperpolarized using PHIP [81]. Recently, real-time metabolism of the molecule has been demonstrated *in vivo* [144]. Furthermore, succinate can induce hypertension in animals when administered intravenously [145]; it is unclear whether this effect occurs in humans, but if it does, this may limit its clinical application.

[1-^{13}C]-α-ketoisocaproate

α-Ketoisocaproate (KIC) is metabolized to leucine by the enzyme branched-chain amino acid transferase (BCAT), which is found to be upregulated in some tumors. BCAT is a putative marker for metastasis and a target for the proto-oncogene c-myc. Injection of hyperpolarized [1-^{13}C]KIC into rodents have shown ample conversion into leucine [146]. In a preclinical study, the SNR and contrast were compared between hyperpolarized [1-^{13}C]pyruvate and [1-^{13}C]-KIC. Here, similar imaging abilities between the two substrates were found. [1-^{13}C]KIC showed a 2.5-times lower SNR compared with [1-^{13}C]pyruvate, whereas the contrast was 20% higher. Very different fluxes through the BCAT-catalyzed reaction can be detected for murine lymphoma (EL4) and rat mammary adenocarcioma (R3230AC) tumors *in vivo* [146]. KIC is suitable for the profiling of tumors at the single gene level and introduced as a novel imaging modality for tumors with high BCAT activity.

3,5-Difluorobenzoyl-L-glutamic Acid

Gene-directed enzyme prodrug therapy is a cancer treatment strategy that aims to reduce systemic toxicity by systemically administering a nontoxic prodrug that is converted to the toxic drug in the tumor by a nonendogenous enzyme delivered by viral vectors only to tumor cells. This complex strategy holds considerable promise for reducing dose-limiting systemic toxicity but depends on the successful delivery of the enzyme and the prodrug to the tumor. One enzyme system of interest is the Carboxypeptidase G2 (CPG2) bacterial enzyme system [147]. A hyperpolarized reporter probe has been developed, 3,5-difluorobenzoyl-L-glutamic acid (3,5-DFBGlu), which is a substrate for CPG2, and has been shown to report on CPGT enzyme activity *in vitro* [97].

^{13}C-choline and ^{15}N-choline

Malignant transformation of cells is characterized by increased phosphocholine concentrations, and studies of both ^{1}H and ^{31}P MRS have demonstrated elevated levels of this metabolite in many different forms of tumor compared with the normal tissue [148]. ^{13}C-labeled choline can be polarized, but the carbon T_1's are short because of dipolar interactions with directly bonded hydrogen atoms. ^{15}N-labeled choline can be hyperpolarized, and because it has a long T_1 (~4 minutes), this would make it suitable for imaging [92]. However, the small chemical shift difference between the ^{15}N resonances of choline and phosphocholine (~0.2 ppm) would make them difficult to differentiate *in vivo* at clinical magnetic field strengths. This problem has been addressed by transferring polarization to spin-coupled protons [94]. However, as yet, there seems to be no evidence that the choline kinase–catalyzed phosphorylation of choline is sufficiently rapid, either in cells *in vitro* or in tumors *in vivo*, to produce detectable levels of labeled phosphocholine within the lifetime of the polarization.

Constraints on Translation to Clinical Application

A number of hurdles to the clinical translation of hyperpolarized methods must be overcome. These hurdles relate to technical and practical issues associated with the components of the MR scanner and the polarizer, concerns about safety of the hyperpolarized substrate, and the challenges of developing well-validated, standardized protocols useful across multiple centers. There are numerous other relevant issues related to the commercialization of this technology, but these topics are beyond the scope of this report.

MR Scanner Software and Hardware Constraints

Because the frequencies for ^{13}C and ^{15}N differ significantly from that used for conventional ^{1}H imaging, the radiofrequency hardware including transmitters, receivers, filters, and amplifiers all need to be tuned to these specific frequencies. Also, the spatial localization necessary for ^{13}C and ^{15}N MRS and MRI inherently is more demanding than conventional ^{1}H MR. This is because of the significantly lower γ for these nuclei, therefore requiring ~16× and 100× more gradient power to achieve the same spatial resolution for ^{13}C and ^{15}N, respectively. Although clinical MR scanners are typically proton-only systems, MR manufacturers have provided multinuclear capabilities for many years and can certainly overcome the previously mentioned constraints. Decoupling is also not essential for hyperpolarization applications because it provides only minor signal gains compared with that of hyperpolarization itself, although it will provide a sharpening of hyperpolarized resonances that are coupled to protons [149] with the challenge of remaining within SAR limitations. New pulse sequence developments are required because the properties of hyperpolarized agents are inherently different from endogeneous nonhyperpolarized molecules as described in the Physiology and Metabolism in Preclinical Models section. However, most of the fast ^{13}C MRSI pulse sequences that have been developed for preclinical studies are directly translatable to clinical MR scanners and patient studies. Finally, the design and construction of new specialized radiofrequency coils for ^{13}C and ^{1}H excitation and reception suitable for future human studies is required (Figure 4). Radiofrequency coils for ^{13}C (and other nuclei) have historically been custom made by smaller companies and laboratory built but would need to be provided for hyperpolarized clinical studies by, or in collaboration with, the MR manufacturer.

Generating Hyperpolarized Material with a Sufficiently Long T_1

A critical need is developing polarizer equipment that can conveniently generate a hyperpolarized sample. The requirements for this equipment can be summarized as follows. The polarized product must be sterile and at an acceptable temperature and pH. The material must be free (and proven to be free) from any radical used during the polarization process. The product must be delivered to the subject with a delay of less than 20 seconds to limit signal lost due to relaxation. Such an instrument should provide multiple samples in a timely manner with high polarization and reproducibility. For clinical applications, polarizers must be designed to allow siting close to the clinical MR scanner for facilitated delivery of the hyperpolarized probe.

Although having a sufficiently long T_1 is a significant challenge for the clinical translation of hyperpolarized MR, it is already clear that the hyperpolarized probes that have been used successfully so far in preclinical studies can provide unique and important clinical information with regard to disease diagnosis, prognosis, and treatment response (Conclusions and Recommendations section). Hyperpolarized probes used to date have taken advantage of the longer T_1's of low γ nuclei such as ^{13}C and ^{15}N and by placing the ^{13}C and ^{15}N label in a chemical environment without directly bonded protons. Replacing protons (^{1}H)

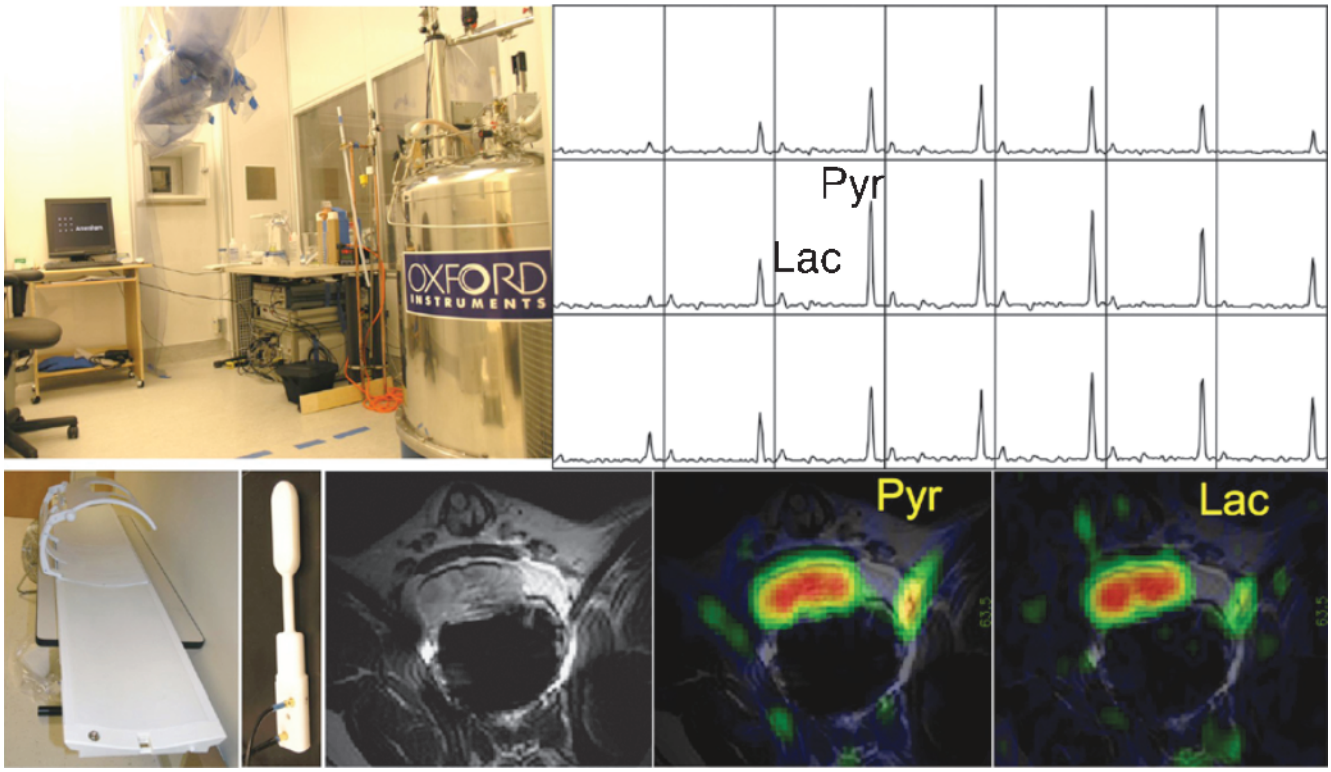

Figure 4. Prototype polarizer (top left) has been installed in a clean room adjacent to a 3-T clinical MR scanner in preparation for a phase 1 clinical trial of [1-^{13}C]pyruvate in prostate cancer patients. The ^{13}C/^{1}H coil designs shown (bottom left) are those that will be used in the patient studies. These coils have been tested in canine studies and provided the ^{13}C MRSI data shown on the right. On the top right is a representative canine prostate ^{13}C MRSI array obtained after injection of hyperpolarized [1-^{13}C]pyruvate dose volume of 1.4 ml/kg of body weight, a dose that was determined to be safe in healthy human volunteer studies. The corresponding [1-^{13}C]pyruvate and [1-^{13}C]lactate images overlaid on a axial T_2-weighted image of the canine prostate is shown on the bottom right. The ^{13}C MRSI data were collected in 15 seconds at a spatial resolution of 0.125 cm^3 demonstrating high levels of [1-^{13}C]pyruvate (SNR, ≥200) and lower [1-^{13}C]lactate levels consistent with normal canine prostate tissue metabolism (right). These preliminary MR metabolic imaging studies demonstrated that the T_1 of hyperpolarized [1-^{13}C]pyruvate was sufficient to allow delivery to the prostate and metabolism in a large animal. In addition, there was sufficient sensitivity to detect metabolism throughout the prostate at a much greater spatial and temporal resolution than previously possible with other MR metabolic imaging techniques. Figure adapted from Nelson et al. [153].

with deuterons (^{2}H) in a molecule can also prolong ^{13}C T_1's, but the magnitude of this effect depends on the molecule and the site of the ^{13}C/^{15}N label. Longer-lived hyperpolarized probes can also be created by exploiting molecular symmetry to store spin populations in states (singlet-state) that are inherently isolated and have dramatically longer T_1 relaxation times [87–90,150,151]. Other approaches for lengthening hyperpolarized probe T_1's are also being investigated. One such approach uses hyperpolarized ^{13}C or ^{15}N sites to store hyperpolarization, whereas the MR signal is detected through polarization transfer (e.g., insensitive nuclear enhancement by polarization transfer) to J-coupled protons [83,94]. Another approach uses a reactive molecule that hyperpolarizes well and has a relatively long T_1 to chemically "tag" biomolecules of interest with the longer-lived hyperpolarized label [152]. However, the fundamental upper limits of achievable T_1 times *in vivo* using these approaches are an area of active research.

For patient studies, the probe needs to have a sufficient T_1 relaxation time to overcome the longer blood circulation time of patients relative to preclinical animal models. On the basis of preclinical large animal studies of hyperpolarized [1-^{13}C]pyruvate, its *in vivo* T_1 relaxation time was sufficiently long to be delivered to and metabolized in the canine prostate [153] (Figure 4). The delivery time of gadolinium-based contrast agents to the human prostate (enhancement onset ≈ 15 seconds after the start of injection) suggests that this will also be true of hyperpolarized [1-^{13}C]pyruvate studies in patients [154]. However, such T_1 relaxation time assessments will need to be performed on all new hyperpolarized probes.

Safety of the Agent

In many cases, the molecules currently under study—pyruvate, bicarbonate, lactate, and others—are products of normal intermediary metabolism and are normally present *in vivo*. Hence, the molecules themselves are inherently safe, and there is an enormous knowledge base about their metabolism as well as their effects in mammals including humans. However, current hyperpolarization methods require that a significant amount of hyperpolarized material must be delivered. Consequently, unlike PET, it is possible that the hyperpolarized substrate itself will influence metabolic processes. The potential physiological consequences of the hyperpolarized substrate must also be carefully evaluated, and this evaluation is an important focus of current research. Hyperpolarized [1-^{13}C]pyruvate, for example, is being developed for clinical studies of prostate cancer. In preparation for human studies, initial dose-escalation safety and tolerability studies were performed in rats, in anesthetized and conscious dogs (Figure 4), and nonhyperpolarized [1-^{13}C]pyruvate in human volunteers [155]. To date, no

significant adverse effects have been observed, and hyperpolarized [1-^{13}C]pyruvate has Investigational New Drug approval for initial use in prostate cancer patients, with a phase 1 clinical trial poised to begin.

Standardized Protocols

The translation of high-end imaging techniques into clinical practice requires the development and optimization of imaging protocols, establishing quality assurance and standardization protocols and sufficient patient studies necessary to establish the best clinical applications of the technology [156]. In many respects, hyperpolarized science will need to repeat many of the evaluation protocols that were developed for understanding the relative roles of other imaging modalities. The development and validation of the new and emerging imaging technologies for clinical research and practice, such as hyperpolarized imaging methods, pose new problems that require broad expertise and resources to solve. The translation process requires not only basic technique development and integration on commercial platforms but also patient validation studies necessary to adequately demonstrate the clinical value of the new imaging technique and to establish robust acquisition and analysis protocols. The clinical translation of hyperpolarized imaging techniques could therefore benefit greatly from the help of groups such as the National Institutes of Health (NIH) Translational Research Working Group whose mandate is to help integrate the complementary skills and expertise of both academic institutions and industry to jointly pursue specific early stage product development opportunities [156].

Conclusions and Recommendations

For many years, it has been known that tumor metabolism differs dramatically from normal tissues in many respects. The advent of molecular methods has illuminated the links between oncogenes and metabolic activity, and the recently introduced concept that some cancers arise as a consequence of abnormal metabolism has generated intense interest. Although the detection of hyperpolarized nuclei in biologic systems is relatively recent, it is already established that MRI of hyperpolarized nuclei, particularly ^{13}C, provides information that is intrinsically not available using current molecular imaging methods. This information—the detection of metabolism in individual enzyme-catalyzed reactions—offers a fundamentally new approach to imaging and understanding cancer biology in both primary and metastatic lesions. Furthermore, despite the relatively limited data available from *in vivo* studies, there are no obvious issues that prohibit translation to humans. In view of this opportunity for improved imaging and the need for improved imaging of primary and metastatic cancers, we have a number of recommendations.

First, hyperpolarized MR studies would greatly benefit from further work focused on better understanding correlations between enzyme-catalyzed reactions and malignancy. Many fundamental questions are involved: What are the most informative reactions or pathways? Which reactions are most sensitive to therapy? Which reactions correlate with prognosis? This effort could but does not necessarily involve hyperpolarization in the early stages; a number of methods are suitable for probing metabolism in cells and animal models. This effort, of course, could immediately involve integration of hyperpolarization techniques with standard methods for measuring metabolic fluxes in cell and animal models. Numerous aspects of cancer biology—early detection of cancers and diseases, characterization of tumor microenvironments, prediction of disease severity and cancer outcome, evaluation of therapeutic responses, and others—could be the targets of this effort.

Second, technology should be developed for efficient, convenient, and reproducible and cost-effective production of large quantities of highly polarized materials. Methods to store polarizations for prolonged periods should be investigated.

Third, there is a need for development of new agents enriched with either ^{13}C or ^{15}N that combine two features: long T_1 of the hyperpolarized nucleus and rapid entry into meaningful biochemical pathways. This effort will require strong collaboration between synthetic chemists and biochemists with expertise in intermediary metabolism.

Fourth, at this early stage in its development, the MR community has the opportunity to develop coherent strategies to standardize and harmonize methods for hyperpolarized MR data acquisition and display. Common protocols for quality assurance, calibration, software for data analysis, and others are all important objectives. Ideally, these methods are independent of the imaging platform.

Fifth, the rapid development of hyperpolarized MR methods will require involvement from multiple sites and multiple research teams. The opportunity exists to foster academic and industry collaborations through polarizers and large-animal systems at multiple research sites.

Finally, it is important for imaging researchers to develop a consensus on how to validate these emerging HP methods to help accelerate clinical research.

This report generated from a wide range of researchers and imaging physicians is a reflection of a strong interest by the research community in moving this important new imaging method forward to address the cancer problem and other diseases. It is difficult to imagine the relatively primitive state of clinical imaging, less than 40 years ago, when a "staging laparotomy" was a state-of-the-art diagnostic method practiced at the most advanced oncology centers. Each technology that we now take for granted required strong collaborations across multiple disciplines and the investment of significant resources. Progress in basic physics and chemistry again presents the medical and scientific community with an opportunity to fundamentally improve clinical imaging of cancer.

Acknowledgments

This report was initiated through discussions with representatives of the National Cancer Institute (NCI) Cancer Imaging Program and other NIH extramural programs (National Institute of Diabetes and Digestive and Kidney Diseases; National Heart, Lung, and Blood Institute; National Institute of Biomedical Imaging and Bioengineering; and National Center for Research Resources). The initial draft was reviewed and edited by more than 60 scientists, followed by extensive discussions at a workshop at the International Society for Magnetic Resonance in Medicine meeting in May 2010 with more than 40 scientists from academia, industry, and federal agencies from the United States and other countries. The authors appreciate the assistance from NIH extramural program staff Huiming Zhang, Maren Laughlin, Guoying Liu, Narasimhan Danthi, Abraham Levy, Gary Kelloff, James Tatum, and Larry Clarke during the development of this report and for organizing the workshop. The authors would also like to thank other contributors, namely Stephen Russek from the National Institute of Standards and Technology, Murali C. Krishna from NCI intramural, and the editorial review of this report suggested by NCI by Craig Thompson from the University of Pennsylvania and Jeffrey Evelhoch from Merck. The authors thank several UK investigators who participated in this publication as part of a National Cancer Institute and Cancer Research United Kingdom collaboration.

References

[1] Deberardinis RJ, Sayed N, Ditsworth D, and Thompson CB (2008). Brick by brick: metabolism and tumor cell growth. *Curr Opin Genet Dev* **18**(1), 54–61.

[2] Kaelin WG Jr and Thompson CB (2010). Q&A: cancer: clues from cell metabolism. *Nature* **465**(7298), 562–564.

[3] Warburg O (1956). On the origin of cancer cells. *Science* **123**(3191), 309–314.

[4] Warburg O, Wind F, and Negelein E (1926). Uber den Stoffwechsel von Tumouren im Korper. *Klin Woch* **5**, 829–832.

[5] Altenberg B and Greulich KO (2004). Genes of glycolysis are ubiquitously overexpressed in 24 cancer classes. *Genomics* **84**(6), 1014–1020.

[6] Sauer LA, Stayman JW III, and Dauchy RT (1982). Amino acid, glucose, and lactic acid utilization *in vivo* by rat tumors. *Cancer Res* **42**(10), 4090–4097.

[7] Kuhajda FP (2000). Fatty-acid synthase and human cancer: new perspectives on its role in tumor biology. *Nutrition* **16**(3), 202–208.

[8] Ookhtens M, Kannan R, Lyon I, and Baker N (1984). Liver and adipose tissue contributions to newly formed fatty acids in an ascites tumor. *Am J Physiol* **247** (1 pt 2), R146–R153.

[9] Swinnen JV, Brusselmans K, and Verhoeven G (2006). Increased lipogenesis in cancer cells: new players, novel targets. *Curr Opin Clin Nutr Metab Care* **9**(4), 358–365.

[10] Gillies RJ, Raghunand N, Garcia-Martin ML, and Gatenby RA (2004). pH imaging. A review of pH measurement methods and applications in cancers. *IEEE Eng Med Biol Mag* **23**(5), 57–64.

[11] Raghunand N, He X, van Sluis R, Mahoney B, Baggett B, Taylor CW, Paine-Murrieta G, Roe D, Bhujwalla ZM, and Gillies RJ (1999). Enhancement of chemotherapy by manipulation of tumour pH. *Br J Cancer* **80**, 1005–1011.

[12] Raghunand N, Mahoney B, van Sluis R, Baggett B, and Gillies RJ (2001). Acute metabolic alkalosis enhances response of C3H mouse mammary tumors to the weak base mitoxantrone. *Neoplasia* **3**, 227–235.

[13] Baysal BE, Ferrell RE, Willett-Brozick JE, Lawrence EC, Myssiorek D, Bosch A, van der Mey A, Taschner PE, Rubinstein WS, Myers EN, et al. (2000). Mutations in *SDHD*, a mitochondrial complex II gene, in hereditary paraganglioma. *Science* **287**(5454), 848–851.

[14] Grinstein S, Swallow CJ, and Rotstein OD (1991). Regulation of cytoplasmic pH in phagocytic cell function and dysfunction. *Clin Biochem* **24**(3), 241–247.

[15] Kim JW, Tchernyshyov I, Semenza GL, and Dang CV (2006). HIF-1–mediated expression of pyruvate dehydrogenase kinase: a metabolic switch required for cellular adaptation to hypoxia. *Cell Metab* **3**(3), 177–185.

[16] Matoba S, Kang JG, Patino WD, Wragg A, Boehm M, Gavrilova O, Hurley PJ, Bunz F, and Hwang PM (2006). p53 regulates mitochondrial respiration. *Science* **312**(5780), 1650–1653.

[17] Flier JS, Mueckler MM, Usher P, and Lodish HF (1987). Elevated levels of glucose transport and transporter messenger RNA are induced by *ras* or *src* oncogenes. *Science* **235**(4795), 1492–1495.

[18] Gao P, Tchernyshyov I, Chang TC, Lee YS, Kita K, Ochi T, Zeller KI, De Marzo AM, Van Eyk JE, Mendell JT, et al. (2009). c-Myc suppression of miR-23a/b enhances mitochondrial glutaminase expression and glutamine metabolism. *Nature* **458**(7239), 762–765.

[19] Shim H, Dolde C, Lewis BC, Wu CS, Dang G, Jungmann RA, Dalla-Favera R, and Dang CV (1997). c-Myc transactivation of LDH-A: implications for tumor metabolism and growth. *Proc Natl Acad Sci USA* **94**(13), 6658–6663.

[20] Wise DR, De Berardinis RJ, Mancuso A, Sayed N, Zhang XY, Pfeiffer HK, Nissim I, Daikhin E, Yudkoff M, McMahon SB, et al. (2008). Myc regulates a transcriptional program that stimulates mitochondrial glutaminolysis and leads to glutamine addiction. *Proc Natl Acad Sci USA* **105**(48), 18782–18787.

[21] Kawauchi K, Araki K, Tobiume K, and Tanaka N (2008). p53 regulates glucose metabolism through an IKK–NF-κB pathway and inhibits cell transformation. *Nat Cell Biol* **10**(5), 611–618.

[22] Astuti D, Latif F, Dallol A, Dahia PL, Douglas F, George E, Skoldberg F, Husebye ES, Eng C, and Maher ER (2001). Gene mutations in the succinate dehydrogenase subunit SDHB cause susceptibility to familial pheochromocytoma and to familial paraganglioma. *Am J Hum Genet* **69**(1), 49–54.

[23] Niemann S and Muller U (2000). Mutations in SDHC cause autosomal dominant paraganglioma, type 3. *Nat Genet* **26**(3), 268–270.

[24] Selak MA, Armour SM, MacKenzie ED, Boulahbel H, Watson DG, Mansfield KD, Pan Y, Simon MC, Thompson CB, and Gottlieb E (2005). Succinate links TCA cycle dysfunction to oncogenesis by inhibiting HIF-α prolyl hydroxylase. *Cancer Cell* **7**(1), 77–85.

[25] Mardis ER, Ding L, Dooling DJ, Larson DE, McLellan MD, Chen K, Koboldt DC, Fulton RS, Delehaunty KD, McGrath SD, et al. (2009). Recurring mutations found by sequencing an acute myeloid leukemia genome. *N Engl J Med* **361**(11), 1058–1066.

[26] Parsons DW, Jones S, Zhang X, Lin JC, Leary RJ, Angenendt P, Mankoo P, Carter H, Siu IM, Gallia GL, et al. (2008). An integrated genomic analysis of human glioblastoma multiforme. *Science* **321**(5897), 1807–1812.

[27] Yan H, Parsons DW, Jin G, McLendon R, Rasheed BA, Yuan W, Kos I, Batinic-Haberle I, Jones S, Riggins GJ, et al. (2009). IDH1 and IDH2 mutations in gliomas. *N Engl J Med* **360**(8), 765–773.

[28] Dang L, White DW, Gross S, Bennett BD, Bittinger MA, Driggers EM, Fantin VR, Jang HG, Jin S, Keenan MC, et al. (2009). Cancer-associated IDH1 mutations produce 2-hydroxyglutarate. *Nature* **462**(7274), 739–744.

[29] Langbein S, Zerilli M, Zur Hausen A, Staiger W, Rensch-Boschert K, Lukan N, Popa J, Ternullo MP, Steidler A, Weiss C, et al. (2006). Expression of transketolase TKTL1 predicts colon and urothelial cancer patient survival: Warburg effect reinterpreted. *Br J Cancer* **94**(4), 578–585.

[30] Krockenberger M, Honig A, Rieger L, Coy JF, Sutterlin M, Kapp M, Horn E, Dietl J, and Kammerer U (2007). Transketolase-like 1 expression correlates with subtypes of ovarian cancer and the presence of distant metastases. *Int J Gynecol Cancer* **17**(1), 101–106.

[31] Christofk HR, Vander Heiden MG, Harris MH, Ramanathan A, Gerszten RE, Wei R, Fleming MD, Schreiber SL, and Cantley LC (2008). The M2 splice isoform of pyruvate kinase is important for cancer metabolism and tumour growth. *Nature* **452**(7184), 230–233.

[32] Fantin VR, St-Pierre J, and Leder P (2006). Attenuation of LDH-A expression uncovers a link between glycolysis, mitochondrial physiology, and tumor maintenance. *Cancer Cell* **9**(6), 425–434.

[33] Hatzivassiliou G, Zhao F, Bauer DE, Andreadis C, Shaw AN, Dhanak D, Hingorani SR, Tuveson DA, and Thompson CB (2005). ATP citrate lyase inhibition can suppress tumor cell growth. *Cancer Cell* **8**(4), 311–321.

[34] Sonveaux P, Vegran F, Schroeder T, Wergin MC, Verrax J, Rabbani ZN, De Saedeleer CJ, Kennedy KM, Diepart C, Jordan BF, et al. (2008). Targeting lactate-fueled respiration selectively kills hypoxic tumor cells in mice. *J Clin Invest* **118**(12), 3930–3942.

[35] Mankoff DA (2007). A definition of molecular imaging. *J Nucl Med* **48**(6), 18N, 21N.

[36] Blodgett TM, Meltzer CC, and Townsend DW (2007). PET/CT: form and function. *Radiology* **242**(2), 360–385.

[37] Breeuwsma AJ, Pruim J, van den Bergh AC, Leliveld AM, Nijman RJ, Dierckx RA, and de Jong IJ (2009). Detection of local, regional, and distant recurrence in patients with PSA relapse after external-beam radiotherapy using (11)C-choline positron emission tomography. *Int J Radiat Oncol Biol Phys* **77**, 160–164.

[38] Piert M, Park H, Khan A, Siddiqui J, Hussain H, Chenevert T, Wood D, Johnson T, Shah RB, and Meyer C (2009). Detection of aggressive primary prostate cancer with ^{11}C-choline PET/CT using multimodality fusion techniques. *J Nucl Med* **50**(10), 1585–1593.

[39] Talbot JN, Gutman F, Fartoux L, Grange JD, Ganne N, Kerrou K, Grahek D, Montravers F, Poupon R, and Rosmorduc O (2006). PET/CT in patients with hepatocellular carcinoma using [(18)F]fluorocholine: preliminary comparison with [(18)F]FDG PET/CT. *Eur J Nucl Med Mol Imaging* **33**(11), 1285–1289.

[40] Kubota K, Furumoto S, Iwata R, Fukuda H, Kawamura K, and Ishiwata K (2006). Comparison of ^{18}F-fluoromethylcholine and 2-deoxy-D-glucose in the distribution of tumor and inflammation. *Ann Nucl Med* **20**(8), 527–533.

[41] Buck AK, Herrmann K, Shen C, Dechow T, Schwaiger M, and Wester HJ (2009). Molecular imaging of proliferation *in vivo*: positron emission tomography with [^{18}F]fluorothymidine. *Methods* **48**(2), 205–215.

[42] Buchmann I, Henze M, Engelbrecht S, Eisenhut M, Runz A, Schafer M, Schilling T, Haufe S, Herrmann T, and Haberkorn U (2007). Comparison of ^{68}Ga-DOTATOC PET and ^{111}In-DTPAOC (Octreoscan) SPECT in patients with neuroendocrine tumours. *Eur J Nucl Med Mol Imaging* **34**(10), 1617–1626.

[43] Haubner R (2006). $\alpha_v\beta_3$-Integrin imaging: a new approach to characterise angiogenesis? *Eur J Nucl Med Mol Imaging* **33**(suppl 1), 54–63.

[44] Troost EG, Schinagl DA, Bussink J, Boerman OC, van der Kogel AJ, Oyen WJ, and Kaanders JH (2009). Innovations in radiotherapy planning of head and neck cancers: role of PET. *J Nucl Med* **51**(1), 66–76.

[45] Chuang CF, Chan AA, Larson D, Verhey LJ, McDermott M, Nelson SJ, and Pirzkall A (2007). Potential value of MR spectroscopic imaging for the radiosurgical management of patients with recurrent high-grade gliomas. *Technol Cancer Res Treat* **6**(5), 375–382.

[46] Kurhanewicz J and Vigneron DB (2008). Advances in MR spectroscopy of the prostate. *Magn Reson Imaging Clin N Am* **16**(4), 697–710.

[47] Mountford C, Ramadan S, Stanwell P, and Malycha P (2009). Proton MRS of the breast in the clinical setting. *NMR Biomed* **22**(1), 54–64.

[48] Haddadin IS, McIntosh A, Meisamy S, Corum C, Styczynski Snyder AL, Powell NJ, Nelson MT, Yee D, Garwood M, and Bolan PJ (2009). Metabolite quantification and high-field MRS in breast cancer. *NMR Biomed* **22**(1), 65–76.

[49] Nelson SJ, Graves E, Pirzkall A, Li X, Antiniw Chan A, Vigneron DB, and McKnight TR (2002). *In vivo* molecular imaging for planning radiation therapy of gliomas: an application of ^{1}H MRSI. *J Magn Reson Imaging* **16**(4), 464–476.

[50] Gillies RJ and Morse DL (2005). *In vivo* magnetic resonance spectroscopy in cancer. *Annu Rev Biomed Eng* **7**, 287–326.

[51] Geraghty PR, van den Bosch MA, Spielman DM, Hunjan S, Birdwell RL, Fong KJ, Stables LA, Zakhour M, Herfkens RJ, and Ikeda DM (2008). MRI and (1)H MRS of the breast: presence of a choline peak as malignancy marker is related to K21 value of the tumor in patients with invasive ductal carcinoma. *Breast J* **14**(6), 574–580.

[52] Glunde K, Ackerstaff E, Mori N, Jacobs MA, and Bhujwalla ZM (2006). Choline phospholipid metabolism in cancer: consequences for molecular pharmaceutical interventions. *Mol Pharm* **3**(5), 496–506.

[53] Tse GM, Yeung DK, King AD, Cheung HS, and Yang WT (2007). *In vivo* proton magnetic resonance spectroscopy of breast lesions: an update. *Breast Cancer Res Treat* **104**(3), 249–255.

[54] Chen J, Huang SL, Li T, and Chen XL (2006). *In vivo* research in astrocytoma cell proliferation with ^{1}H-magnetic resonance spectroscopy: correlation with histopathology and immunohistochemistry. *Neuroradiology* **48**(5), 312–318.

[55] Magalhaes A, Godfrey W, Shen Y, Hu J, and Smith W (2005). Proton magnetic resonance spectroscopy of brain tumors correlated with pathology. *Acad Radiol* **12**(1), 51–57.

[56] McKnight TR, Lamborn KR, Love TD, Berger MS, Chang S, Dillon WP, Bollen A, and Nelson SJ (2007). Correlation of magnetic resonance spectroscopic and growth characteristics within grades II and III gliomas. *J Neurosurg* **106**(4), 660–666.

[57] Hou XY and Gao PY (2009). Application of ^{1}H-magnetic resonance spectroscopy in differential diagnosis of brain low-grade gliomas and demyelinating diseases. *Zhongguo Yi Xue Ke Xue Yuan Xue Bao* **31**(2), 206–209.

[58] Spampinato MV, Smith JK, Kwock L, Ewend M, Grimme JD, Camacho DL, and Castillo M (2007). Cerebral blood volume measurements and proton MR spectroscopy in grading of oligodendroglial tumors. *AJR Am J Roentgenol* **188**(1), 204–212.

[59] Sardanelli F, Fausto A, and Podo F (2008). MR spectroscopy of the breast. *Radiol Med* **113**(1), 56–64.

[60] Kwock L, Smith JK, Castillo M, Ewend MG, Cush S, Hensing T, Varia M, Morris D, and Bouldin TW (2002). Clinical applications of proton MR spectroscopy in oncology. *Technol Cancer Res Treat* **1**(1), 17–28.

[61] Findlay MP and Leach MO (1994). *In vivo* monitoring of fluoropyrimidine metabolites: magnetic resonance spectroscopy in the evaluation of 5-fluorouracil. *Anticancer Drugs* **5**(3), 260–280.

[62] Lee CP, Payne GS, Oregioni A, Ruddle R, Tan S, Raynaud FI, Eaton D, Campbell MJ, Cross K, Halbert G, et al. (2009). A phase I study of the nitroimidazole hypoxia marker SR4554 using ^{19}F magnetic resonance spectroscopy. *Br J Cancer* **101**(11), 1860–1868.

[63] Beloueche-Babari M, Chung YL, Al-Saffar NM, Falck-Miniotis M, and Leach MO (2010). Metabolic assessment of the action of targeted cancer therapeutics using magnetic resonance spectroscopy. *Br J Cancer* **102**(1), 1–7.

[64] Workman P, Aboagye EO, Chung YL, Griffiths JR, Hart R, Leach MO, Maxwell RJ, McSheehy PM, Price PM, and Zweit J (2006). Minimally invasive pharmacokinetic and pharmacodynamic technologies in hypothesis-testing clinical trials of innovative therapies. *J Natl Cancer Inst* **98**(9), 580–598.

[65] Kurhanewicz J, Bok R, Nelson SJ, and Vigneron DB (2008). Current and potential applications of clinical ^{13}C MR spectroscopy. *J Nucl Med* **49**(3), 341–344.

[66] Elstrom RL, Bauer DE, Buzzai M, Karnauskas R, Harris MH, Plas DR, Zhuang H, Cinalli RM, Alavi A, Rudin CM, et al. (2004). Akt stimulates aerobic glycolysis in cancer cells. *Cancer Res* **64**(11), 3892–3899.

[67] Gardner LB, Li Q, Park MS, Flanagan WM, Semenza GL, and Dang CV (2001). Hypoxia inhibits G_1/S transition through regulation of p27 expression. *J Biol Chem* **276**(11), 7919–7926.

[68] Aime S, Dastru W, Gobetto R, Santelia D, and Viale A (2008). Agents for polarization enhancement in MRI. In *Molecular Imaging, Handbook of Experimental Pharmacology.* Vol 185/I. W Semmler and M Schwaiger (Eds). Springer-Verlag, Berlin, Germany. pp. 248–269.

[69] Ardenkjaer-Larsen JH (2009). Hyperpolarized ^{13}C magnetic resonance imaging—principles and applications. In *Molecular Imaging: Principles and Practice*. People's Medical Publishing House, Shelton, CT. pp. 377–388.

[70] Bhattacharya P, Ross BD, and Bunger R (2009). Cardiovascular applications of hyperpolarized contrast media and metabolic tracers. *Exp Biol Med (Maywood)* **234**(12), 1395–1416.

[71] Brindle K (2008). New approaches for imaging tumour responses to treatment. *Nat Rev Cancer* **8**, 1–14.

[72] Albert MS, Cates GD, Driehuys B, Happer W, Saam B, Springer CS Jr, and Wishnia A (1994). Biological magnetic resonance imaging using laser-polarized ^{129}Xe. *Nature* **370**(6486), 199–201.

[73] Ebert M, Grossmann T, Heil W, Otten WE, Surkau R, Leduc M, Bachert P, Knopp MV, Schad LR, and Thelen M (1996). Nuclear magnetic resonance imaging with hyperpolarised helium-3. *Lancet* **347**(9011), 1297–1299.

[74] Fischer MC, Spector ZZ, Ishii M, Yu J, Emami K, Itkin M, and Rizi R (2004). Single-acquisition sequence for the measurement of oxygen partial pressure by hyperpolarized gas MRI. *Magn Reson Med* **52**(4), 766–773.

[75] Mata JF, Altes TA, Cai J, Ruppert K, Mitzner W, Hagspiel KD, Patel B, Salerno M, Brookeman JR, de Lange EE, et al. (2007). Evaluation of emphysema severity and progression in a rabbit model: comparison of hyperpolarized ^{3}He and ^{129}Xe diffusion MRI with lung morphometry. *J Appl Physiol* **102**(3), 1273–1280.

[76] Rizi RR, Dimitrov IE, Thompson A, Jones G, Gentile TR, Ishii M, Reddy R, Schnall MD, and Leigh JS (1998). MRI of hyperpolarized ^{3}He gas in human paranasal sinuses. *Magn Reson Med* **39**(6), 865–868.

[77] Bowers CR and Weitekamp DP (1986). Transformation of symmetrization order to nuclear-spin magnetization by chemical reaction and nuclear magnetic resonance. *Phys Rev Lett* **57**(21), 2645–2648.

[78] Bowers CR and Weitekamp DP (1987). Parahydrogen and synthesis allow dramatically enhanced nuclear alignment. *J Am Chem Soc* **109**, 5541–5542.

[79] Abragam A and Goldman M (1978). Principles of dynamic nuclear polarisation. *Rep Prog Phys* **41**(3), 395–399.

[80] Ardenkjaer-Larsen JH, Fridlund B, Gram A, Hansson G, Hansson L, Lerche MH, Servin R, Thaning M, and Golman K (2003). Increase in signal-to-noise ratio of >10,000 times in liquid-state NMR. *Proc Natl Acad Sci USA* **100**(18), 10158–10163.

[81] Chekmenev EY, Hovener J, Norton VA, Harris K, Batchelder LS, Bhattacharya P, Ross BD, and Weitekamp DP (2008). PASADENA hyperpolarization of succinic acid for MRI and NMR spectroscopy. *J Am Chem Soc* **130**(13), 4212–4213.

[82] Goldman M, Jóhannesson H, Axelsson O, and Karlsson M (2005). Hyperpolarization of ^{13}C through order transfer from parahydrogen: a new contrast agent for MRI. *Magn Reson Imaging* **23**(2), 153–157.

[83] Chekmenev EY, Norton VA, Weitekamp DP, and Bhattacharya P (2009). Hyperpolarized (1)H NMR employing low γ nucleus for spin polarization storage. *J Am Chem Soc* **131**(9), 3164–3165.

[84] Adams RW, Aguilar JA, Atkinson KD, Cowley MJ, Elliott PI, Duckett SB, Green GG, Khazal IG, Lopez-Serrano J, and Williamson DC (2009). Reversible interactions with para-hydrogen enhance NMR sensitivity by polarization transfer. *Science* **323**(5922), 1708–1711.

[85] Atkinson KD, Cowley MJ, Elliott PI, Duckett SB, Green GG, Lopez-Serrano J, and Whitwood AC (2009). Spontaneous transfer of parahydrogen derived spin order to pyridine at low magnetic field. *J Am Chem Soc* **131**(37), 13362–13368.

[86] Adams RW, Duckett SB, Green RA, Williamson DC, and Green GG (2009). A theoretical basis for spontaneous polarization transfer in non-hydrogenative parahydrogen–induced polarization. *J Chem Phys* **131**(19), 194505.

[87] Carravetta M, Johannessen OG, and Levitt MH (2004). Beyond the T_1 limit: singlet nuclear spin states in low magnetic fields. *Phys Rev Lett* **92**(15), 153003.

[88] Carravetta M and Levitt MH (2005). Theory of long-lived nuclear spin states in solution nuclear magnetic resonance. I. Singlet states in low magnetic field. *J Chem Phys* **122**(21), 214505.

[89] Sarkar R, Ahuja P, Moskau D, Vasos PR, and Bodenhausen G (2007). Extending the scope of singlet-state spectroscopy. *Chemphyschem* **8**(18), 2652–2656.

[90] Warren WS, Jenista E, Branca RT, and Chen X (2009). Increasing hyperpolarized spin lifetimes through true singlet eigenstates. *Science* **323**(5922), 1711–1714.

[91] Aptekar JW, Cassidy MC, Johnson AC, Barton RA, Lee M, Ogier AC, Vo C, Anahtar MN, Ren Y, Bhatia SN, et al. (2009). Silicon nanoparticles as hyperpolarized magnetic resonance imaging agents. *ACS Nano* **3**(12), 4003–4008.

[92] Gabellieri C, Reynolds S, Lavie A, Payne GS, Leach MO, and Eykyn TR (2008). Therapeutic target metabolism observed using hyperpolarized ^{15}N choline. *J Am Chem Soc* **130**(14), 4598–4599.

[93] Mishkovsky M and Frydman L (2008). Progress in hyperpolarized ultrafast 2D NMR spectroscopy. *Chemphyschem* **9**(16), 2340–2348.

[94] Sarkar R, Comment A, Vasos PR, Jannin S, Gruetter R, Bodenhausen G, Hall H, Kirik D, and Denisov VP (2009). Proton NMR of (15)N-choline metabolites enhanced by dynamic nuclear polarization. *J Am Chem Soc* **131**(44), 16014–16015.

[95] van Heeswijk RB, Uffmann K, Comment A, Kurdzesau F, Perazzolo C, Cudalbu C, Jannin S, Konter JA, Hautle P, van den Brandt B, et al. (2009). Hyperpolarized lithium-6 as a sensor of nanomolar contrast agents. *Magn Reson Med* **61**(6), 1489–1493.

[96] Wolber J, Ellner F, Fridlund B, Gram A, Johannesson H, Hansson G, Hansson LH, Lerche MH, Mansson S, Servin R, et al. (2004). Generating highly polarized nuclear spins in solution using dynamic nuclear polarization. *Nucl Instrum Meth A* **526**(1–2), 173–181.

[97] Jamin Y, Gabellieri C, Smyth L, Reynolds S, Robinson SP, Springer CJ, Leach MO, Payne GS, and Eykyn TR (2009). Hyperpolarized (13)C magnetic resonance detection of carboxypeptidase G2 activity. *Magn Reson Med* **62**(5), 1300–1304.

[98] Comment A, Rentsch J, Kurdzesau F, Jannin S, Uffmann K, van Heeswijk RB, Hautle P, Konter JA, van den Brandt B, and van der Klink JJ (2008). Producing over 100 ml of highly concentrated hyperpolarized solution by means of dissolution DNP. *J Magn Reson* **194**(1), 152–155.

[99] Jannin S, Comment A, Kurdzesau F, Konter JA, Hautle P, van den Brandt B, and van der Klink JJ (2008). A 140 GHz prepolarizer for dissolution dynamic nuclear polarization. *J Chem Phys* **128**(24), 241102.

[100] Johannesson H, Macholl S, and Ardenkjaer-Larsen JH (2009). Dynamic nuclear polarization of [1-^{13}C]pyruvic acid at 4.6 tesla. *J Magn Reson* **197**(2), 167–175.

[101] McCarney ER, Armstrong BD, Lingwood MD, and Han S (2007). Hyperpolarized water as an authentic magnetic resonance imaging contrast agent. *Proc Natl Acad Sci USA* **104**(6), 1754–1759.

[102] Merritt ME, Harrison C, Kovacs Z, Kshirsagar P, Malloy CR, and Sherry AD (2007). Hyperpolarized ^{89}Y offers the potential of direct imaging of metal ions in biological systems by magnetic resonance. *J Am Chem Soc* **129**(43), 12942–12943.

[103] Hu S, Lustig M, Chen AP, Crane J, Kerr A, Kelley DA, Hurd R, Kurhanewicz J, Nelson SJ, Pauly JM, et al. (2008). Compressed sensing for resolution enhancement of hyperpolarized ^{13}C flyback 3D-MRSI. *J Magn Reson* **192**(2), 258–264.

[104] Mayer D, Yen YF, Tropp J, Pfefferbaum A, Hurd RE, and Spielman DM (2009). Application of subsecond spiral chemical shift imaging to real-time multislice metabolic imaging of the rat *in vivo* after injection of hyperpolarized ^{13}C1-pyruvate. *Magn Reson Med* **62**(3), 557–564.

[105] Kohler SJ, Yen Y, Wolber J, Chen AP, Albers MJ, Bok R, Zhang V, Tropp J, Nelson S, Vigneron DB, et al. (2007). *In vivo* carbon 13 metabolic imaging at 3T with hyperpolarized ^{13}C-1-pyruvate. *Magn Reson Med* **58**(1), 65–69.

[106] Schroeder MA, Cochlin LE, Heather LC, Clarke K, Radda GK, and Tyler DJ (2008). *In vivo* assessment of pyruvate dehydrogenase flux in the heart using hyperpolarized carbon-13 magnetic resonance. *Proc Natl Acad Sci USA* **105**(33), 12051–12056.

[107] Oros AM and Shah NJ (2004). Hyperpolarized xenon in NMR and MRI. *Phys Med Biol* **49**(20), R105–R153.

[108] Golman K, Ardenaer-Larsen JH, Petersson JS, Mansson S, and Leunbach I (2003). Molecular imaging with endogenous substances. *Proc Natl Acad Sci USA* **100**(18), 10435–10439.

[109] Golman K, in 't Zandt R, and Thaning M (2006). Real-time metabolic imaging. *Proc Natl Acad Sci USA* **103**(30), 11270–11275.

[110] Golman K and Petersson JS (2006). Metabolic imaging and other applications of hyperpolarized ^{13}C. *Acad Radiol* **13**(8), 932–942.

[111] Levin YS, Mayer D, Yen YF, Hurd RE, and Spielman DM (2007). Optimization of fast spiral chemical shift imaging using least squares reconstruction: application for hyperpolarized (13)C metabolic imaging. *Magn Reson Med* **58**(2), 245–252.

[112] Mayer D, Levin YS, Hurd RE, Glover GH, and Spielman DM (2006). Fast metabolic imaging of systems with sparse spectra: application for hyperpolarized ^{13}C imaging. *Magn Reson Med* **56**(4), 932–937.

[113] Chen AP, Albers MJ, Cunningham CH, Kohler SJ, Yen YF, Hurd RE, Tropp J, Bok R, Pauly JM, Nelson SJ, et al. (2007). Hyperpolarized C-13 spectroscopic imaging of the TRAMP mouse at 3T-initial experience. *Magn Reson Med* **58**(6), 1099–1106.

[114] Cunningham CH, Chen AP, Albers MJ, Kurhanewicz J, Hurd RE, Yen YF, Pauly JM, Nelson SJ, and Vigneron DB (2007). Double spin-echo sequence for rapid spectroscopic imaging of hyperpolarized (13)C. *J Magn Reson* **187**(2), 357–362.

[115] Golman K, Petersson JS, Magnusson P, Johansson E, Akeson P, Chai CM, Hansson G, and Månsson S (2008). Cardiac metabolism measured noninvasively by hyperpolarized (13)C MRI. *Magn Reson Med* **59**(5), 1005–1013.

[116] Hu S, Lustig M, Balakrishnan A, Larson PE, Bok R, Kurhanewicz J, Nelson SJ, Goga A, Pauly JM, and Vigneron DB (2010). 3D compressed sensing for highly accelerated hyperpolarized (13)C MRSI with *in vivo* applications to transgenic mouse models of cancer. *Magn Reson Med* **63**(2), 312–321.

[117] Arunachalam A, Whitt D, Fish K, Giaquinto R, Piel J, Watkins R, and Hancu I (2009). Accelerated spectroscopic imaging of hyperpolarized C-13 pyruvate using SENSE parallel imaging. *NMR Biomed* **22**(8), 867–873.

[118] Cunningham CH, Chen AP, Lustig M, Hargreaves BA, Lupo J, Xu D, Kurhanewicz J, Hurd RE, Pauly JM, Nelson SJ, et al. (2008). Pulse sequence for dynamic volumetric imaging of hyperpolarized metabolic products. *J Magn Reson* **193**(1), 139–146.

[119] Meyer CH, Pauly JM, Macovski A, and Nishimura DG (1990). Simultaneous spatial and spectral selective excitation. *Magn Reson Med* **15**(2), 287–304.

[120] Larson PE, Bok R, Kerr AB, Lustig M, Hu S, Chen AP, Nelson SJ, Pauly JM, Kurhanewicz J, and Vigneron DB (2010). Investigation of tumor hyperpolarized [1-(13)C]-pyruvate dynamics using time-resolved multiband RF excitation echo-planar MRSI. *Magn Reson Med* **63**(3), 582–591.

[121] Larson PE, Kerr AB, Chen AP, Lustig MS, Zierhut ML, Hu S, Cunningham CH, Pauly JM, Kurhanewicz J, and Vigneron DB (2008). Multiband excitation pulses for hyperpolarized ^{13}C dynamic chemical-shift imaging. *J Magn Reson* **194**(1), 121–127.

[122] Kettunen MI, Hu D-E, Witney TH, McLaughlin R, Gallagher FA, Bohndiek SE, Day SE, and Brindle KM (2010). Magnetization transfer measurements of exchange between hyperpolarized [1-^{13}C]pyruvate and [1-^{13}C]lactate in a murine lymphoma. *Magn Reson Med* **63**(4), 872–880.

[123] Albers MJ, Bok R, Chen AP, Cunningham CH, Zierhut ML, Zhang VY, Kohler SJ, Tropp J, Hurd RE, Yen YF, et al. (2008). Hyperpolarized ^{13}C lactate, pyruvate, and alanine: noninvasive biomarkers for prostate cancer detection and grading. *Cancer Res* **68**(20), 8607–8615.

[124] Day SE, Kettunen MI, Gallagher FA, Hu D-E, Lerche M, Wolber J, Golman K, Ardenkjaer-Larsen JH, and Brindle KM (2007). Detecting tumor response to treatment using hyperpolarized ^{13}C magnetic resonance imaging and spectroscopy. *Nature Med* **13**, 1382–1387.

[125] Park I, Larson PE, Zierhut ML, Hu S, Bok R, Ozawa T, Kurhanewicz J, Vigneron DB, Vandenberg SR, James CD, et al. (2010). Hyperpolarized ^{13}C magnetic resonance metabolic imaging: application to brain tumors. *Neuro Oncol* **12**(2), 133–144.

[126] Ward CS, Venkatesh HS, Chaumeil MM, Brandes AH, Vancriekinge M, Dafni H, Sukumar S, Nelson SJ, Vigneron DB, Kurhanewicz J, et al. (2010). Noninvasive detection of target modulation following phosphatidylinositol 3-kinase inhibition using hyperpolarized ^{13}C magnetic resonance spectroscopy. *Cancer Res* **70**(4), 1296–1305.

[127] Harris T, Eliyahu G, Frydman L, and Degani H (2009). Kinetics of hyperpolarized ^{13}C1-pyruvate transport and metabolism in living human breast cancer cells. *Proc Natl Acad Sci USA* **106**(43), 18131–18136.

[128] Merritt ME, Harrison C, Storey C, Jeffrey FM, Sherry AD, and Malloy CR (2007). Hyperpolarized ^{13}C allows a direct measure of flux through a single enzyme-catalyzed step by NMR. *Proc Natl Acad Sci USA* **104**(50), 19773–19777.

[129] Merritt ME, Harrison C, Storey C, Sherry AD, and Malloy CR (2008). Inhibition of carbohydrate oxidation during the first minute of reperfusion after brief ischemia: NMR detection of hyperpolarized $^{13}CO_2$ and $H^{13}CO_3$. *Magn Reson Med* **60**(5), 1029–1036.

[130] Schroeder MA, Atherton HJ, Ball DR, Cole MA, Heather LC, Griffin JL, Clarke K, Radda GK, and Tyler DJ (2009). Real-time assessment of Krebs cycle metabolism using hyperpolarized ^{13}C magnetic resonance spectroscopy. *FASEB J* **23**(8), 2529–2538.

[131] Witney T, Kettunen M, Day S, Hu D, Neves A, Gallagher F, Fulton S, and Brindle K (2009). A comparison between radiolabeled fluorodeoxyglucose uptake and hyperpolarized C-13–labeled pyruvate utilization as methods for detecting tumor response to treatment. *Neoplasia* **6**, 574–582.

[132] Matsumoto S, Espey MG, Utsumi H, Devasahayam N, Matsumoto K, Matsumoto A, Hirata H, Wink DA, Kuppusamy P, Subramanian S, et al. (2008). Dynamic monitoring of localized tumor oxygenation changes using RF pulsed electron paramagnetic resonance in conscious mice. *Magn Reson Med* **59**(3), 619–625.

[133] Keshari KR, Kurhanewicz J, Jeffries RE, Wilson DM, Dewar BJ, Van Criekinge M, Zierhut M, Vigneron DB, and Macdonald JM (2010). Hyperpolarized (13)C spectroscopy and an NMR-compatible bioreactor system for the investigation of real-time cellular metabolism. *Magn Reson Med* **63**(2), 322–329.

[134] Zierhut ML, Yen YF, Chen AP, Bok R, Albers MJ, Zhang V, Tropp J, Park I, Vigneron DB, Kurhanewicz J, et al. (2009). Kinetic modeling of hyperpolarized ^{13}C1-pyruvate metabolism in normal rats and TRAMP mice. *J Magn Reson* **202**(1), 85–92.

[135] Hu S, Chen AP, Zierhut ML, Bok R, Yen YF, Schroeder MA, Hurd RE, Nelson SJ, Kurhanewicz J, and Vigneron DB (2009). *In vivo* carbon-13 dynamic MRS and MRSI of normal and fasted rat liver with hyperpolarized ^{13}C-pyruvate. *Mol Imaging Biol* **11**(6), 399–407.

[136] Hurd RE, Yen YF, Mayer D, Chen A, Wilson D, Kohler S, Bok R, Vigneron D, Kurhanewicz J, Tropp J, et al. (2010). Metabolic imaging in the anesthetized rat brain using hyperpolarized [1-^{13}C] pyruvate and [1-^{13}C] ethyl pyruvate. *Magn Reson Med* **63**(5), 1137–1143.

[137] Gallagher FA, Kettunen MI, Day SE, Hu DE, Ardenkjaer-Larsen JH, Zandt R, Jensen PR, Karlsson M, Golman K, Lerche MH, et al. (2008). Magnetic resonance imaging of pH *in vivo* using hyperpolarized ^{13}C-labelled bicarbonate. *Nature* **453**(7197), 940–943.

[138] Jensen PR, Peitersen T, Karlsson M, In 't Zandt R, Gisselsson A, Hansson G, Meier S, and Lerche MH (2009). Tissue-specific short chain fatty acid metabolism and slow metabolic recovery after ischemia from hyperpolarized NMR *in vivo*. *J Biol Chem* **284**(52), 36077–36082.

[139] Gallagher FA, Kettunen MI, Hu DE, Jensen PR, Zandt RI, Karlsson M, Gisselsson A, Nelson SK, Witney TH, Bohndiek SE, et al. (2009). Production of hyperpolarized [1,4-^{13}C2]malate from [1,4-^{13}C2]fumarate is a marker of cell necrosis and treatment response in tumors. *Proc Natl Acad Sci USA* **106**(47), 19801–19806.

[140] Chen AP, Kurhanewicz J, Bok R, Xu D, Joun D, Zhang V, Nelson SJ, Hurd RE, and Vigneron DB (2008). Feasibility of using hyperpolarized [1-^{13}C]lactate as a substrate for *in vivo* metabolic ^{13}C MRSI studies. *Magn Reson Imaging* **26**(6), 721–726.

[141] Gallagher F, Kettunen M, Day S, Lerche M, and Brindle K (2008). ^{13}C magnetic resonance spectroscopy measurements of glutaminase activity in human hepatocellular carcinoma cells using hyperpolarized ^{13}C-labeled glutamine. *Magn Reson Med* **60**, 253–257.

[142] Jensen PR, Peitersen T, Karlsson M, In't Zandt R, Gisselsson A, Hansson G, Meier S, and Lerche MH (2009). Tissue-specific short chain fatty acid metabolism and slow metabolic recovery after ischemia from hyperpolarized NMR *in vivo*. *J Biol Chem* **284**(52), 36077–36082.

[143] Keshari KR, Wilson DM, Chen AP, Bok R, Larson PE, Hu S, Van Criekinge M, Macdonald JM, Vigneron DB, and Kurhanewicz J (2009). Hyperpolarized [2-^{13}C]-fructose: a hemiketal DNP substrate for *in vivo* metabolic imaging. *J Am Chem Soc* **131**(48), 17591–17596.

[144] Ross BD, Bhattacharya P, Wagner S, Tran T, and Sailasuta N (2009). Hyperpolarized MR imaging: neurologic applications of hyperpolarized metabolism. *AJNR Am J Neuroradiol* **31**(1), 24–33.

[145] He W, Miao F, Lin D, Schwandner R, Wang Z, Gao J, Chen J, Tian H, and Ling L (2004). Citric acid cycle intermediates as ligands for orphan G-protein–coupled receptors. *Nature* **429**, 188–193.

[146] Karlsson M, Jensen PR, in 't Zandt R, Gisselsson A, Hansson G, Duus JO, Meier S, and Lerche MH (2010). Imaging of branched chain amino acid metabolism in tumors with hyperpolarized ^{13}C ketoisocaproate. *Int J Cancer* **127**(3), 729–736.

[147] Friedlos F, Lehouritis P, Ogilvie L, Hedley D, Davies L, Bermudes D, King I, Martin J, Marais R, and Springer CJ (2008). Attenuated Salmonella targets prodrug activating enzyme carboxypeptidase G2 to mouse melanoma and human breast and colon carcinomas for effective suicide gene therapy. *Clin Cancer Res* **14**(13), 4259–4266.

[148] Podo F (1999). Tumour phospholipid metabolism. *NMR Biomed* **12**(7), 413–439.

[149] Chen AP, Tropp J, Hurd RE, Van Criekinge M, Carvajal LG, Xu D, Kurhanewicz J, and Vigneron DB (2009). *In vivo* hyperpolarized ^{13}C MR spectroscopic imaging with ^{1}H decoupling. *J Magn Reson* **197**(1), 100–106.

[150] Pileio G, Carravetta M, Hughes E, and Levitt MH (2008). The long-lived nuclear singlet state of ^{15}N-nitrous oxide in solution. *J Am Chem Soc* **130**(38), 12582–12583.

[151] Pileio G and Levitt MH (2009). Theory of long-lived nuclear spin states in solution nuclear magnetic resonance. II. Singlet spin locking. *J Chem Phys* **130**(21), 214501.

[152] Wilson DM, Hurd RE, Keshari K, Van Criekinge M, Chen AP, Nelson SJ, Vigneron DB, and Kurhanewicz J (2009). Generation of hyperpolarized substrates by secondary labeling with [1,1-^{13}C] acetic anhydride. *Proc Natl Acad Sci USA* **106**(14), 5503–5507.

[153] Nelson SJ, Vigneron D, Kurhanewicz J, Chen A, Bok R, and Hurd R (2008). DNP-hyperpolarized C-13 magnetic resonance metabolic imaging for cancer applications. *Appl Magn Reson* **34**(3–4), 533–544.

[154] Noworolski SM, Henry RG, Vigneron DB, and Kurhanewicz J (2005). Dynamic contrast-enhanced MRI in normal and abnormal prostate tissues as defined by biopsy, MRI, and 3D MRSI. *Magn Reson Med* **53**(2), 249–255.

[155] Nelson S, Vigneron D, Kurhanewicz J, Chen AP, Bok R, and Hurd R (2008). DNP-hyperpolarized ^{13}C magnetic resonance metabolic imaging for cancer applications. *Appl Magn Reson* **34**, 533–544.

[156] Dorfman GS, Sullivan DC, Schnall MD, and Matrisian LM (2008). The Translational Research Working Group developmental pathway for image-based assessment modalities. *Clin Cancer Res* **14**(18), 5678–5684.